crystals

MDPI

Review

Progress in Boron Nitride-Based Materials as Catalysts for Energy Storage and Electrochemical Application

Khursheed Ahmad * and Tae Hwan Oh *

School of Chemical Engineering, Yeungnam University, Gyeongsan 38541, Republic of Korea
* Correspondence: khursheed@yu.ac.kr (K.A.); taehwanoh@ynu.ac.kr (T.H.O.)

Abstract: The design and fabrication of energy storage devices and electrochemical sensors are two major research fields. Many research groups are dedicated to the development of high-performance energy storage (super-capacitors) devices and electrochemical sensors for the determination of various substances. Thus, it would be worth summarizing the recent progress in BN and its composites based materials for energy storage and electrochemical sensing applications. Two-dimensional (2D) boron nitride (BN) is a widely used electrode material for optoelectronic and electrochemical applications. Herein, we report the progress on the use of BN and its composite-based electrode materials for the development of energy storage (super-capacitors; SCs) devices and electrochemical sensors. The challenges and future perspectives are also mentioned.

Keywords: boron nitride; composites; energy storage; sensors

1. Introduction

Currently, it is clear that energy crises will be a major challenge for the world in the future due to the increase in global population and energy consumption [1]. Presently, traditional energy sources such as fossil fuels, etc., are being used but their limited availability and negative impacts on the environment have motivated researchers towards the development of modern energy technologies [2]. In this connection, various energy technologies such as solar cells [3], super-capacitors (SCs) [4], batteries [5], hydrogen production [6], and fuel cells [7], etc., have been developed to reduce the dependency on conventional energy resources. In particular, energy storage devices such as SCs may play a vital role and significantly participate in reducing energy-related issues [8]. SCs have received extensive attention because of their ability to fill the gap between conventional capacitors and high-energy batteries [9]. Additionally, the fast charging–discharging capability with long cyclic stability, cost-effectiveness, and excellent reversibility of SCs makes them a suitable candidate for the development of high-performance energy storage devices [10]. Unfortunately, SCs have some drawbacks such as low power density and energy density, which may limit their commercialization. In this regard, various materials have been investigated to obtain a high storage capacity for the electrodes proposed for use in SCs. Based on the charge storage mechanism and electrode materials, SCs can be classified as electric double-layer capacitors (EDLCs) or pseudo-capacitors. Generally, carbon-based electrodes can be used for EDLCs, whereas conducting polymers and metal oxide-based electrodes are promising candidates for the construction of pseudo-capacitors [9,11]. It has been observed from reported articles that metal oxides possess high stability and appropriate electrochemical activity for the fabrication of pseudo-capacitors.

check for updates

Academic Editor: Zongyou Yin

Received: 5 December 2024
Revised: 25 December 2024
Accepted: 27 December 2024
Published: 29 December 2024

Citation: Ahmad, K.; Oh, T.H. Progress in Boron Nitride-Based Materials as Catalysts for Energy Storage and Electrochemical Application. *Crystals* **2025**, *15*, 27. https://doi.org/10.3390/cryst15010027

Copyright: © 2024 by the authors. Licensee MDPI, Basel, Switzerland. This article is an open access article distributed under the terms and conditions of the Creative Commons Attribution (CC BY) license (https://creativecommons.org/licenses/by/4.0/).

Metal oxides such as zinc oxide (ZnO) [12], manganese dioxide (MnO_2) [13], nickel oxide (NiO) [14], copper oxide (Cu_2O) [15], cobalt oxide (Co_3O_4) [16], tin oxide (SnO_2) [17], molybdenum oxide (MoO_3) [18], and tungsten trioxide (WO_3) [19], etc., have been explored as electrode modifiers for SCs. The metal oxides may exhibit synergistic interactions, which may further improve the capacitance of the fabricated electrodes for SCs. It is understood that the electrochemical properties of the electrode material have a significant role in SCs applications. Similarly, such electrodes can be employed as sensors for the determination of various analytes [20]. Electrochemical sensor technology has also received enormous interest due to its cost effectiveness, fast and simple working principle, excellent selectivity, sensitivity, and stability compared to the conventional sensing technology [21]. Electrochemical sensors are widely used for the determination of various toxic, hazardous, pharmaceutical, and biomolecular substances [22,23]. The sensing activities of the electrodes are influenced by the physicochemical properties of the electrode modifiers. In this context, various electrode modifiers such as ZnO [24], MnO_2 [25], SnO_2 [26], cerium dioxide (CeO_2) [27], NiO [28], Cu_2O [29], and molybdenum disulfide (MoS_2) [30], etc., have been adopted for electrochemical sensing applications. Although, metal oxides are widely explored as energy storage and sensing materials, the low conductivity of the metal oxides is one of the major challenges which needs to be overcome for their practical application.

Boron nitride (BN) is a well-known ceramic material which has a layered structure and exhibits excellent physicochemical properties such as thermal stability, high surface area, mechanical strength, conductivity, and electrochemical properties [31]. In BN, equal numbers of B and N atoms are alternately linked. BN is a material which exists in several forms such as hexagonal BN (h-BN or hBN) and forms an sp^2-bonded configuration which is almost similar to graphite [32]. Other forms of BN are hard cubic BN (c-BN) and amorphous BN (a-BN), which are similar to diamond and amorphous carbon, respectively [33]. It is of great significance to combine BN with other materials to further enhance the electrochemical behavior of the hybrid materials for electrochemical devices. Previously, BN-based materials were explored for dye-sensitized solar cells [34], photo-catalysis [35], hydrogen production [36], metal ion batteries and hydrogen storage [37], oxygen reduction reaction [38], and proton-exchange membrane fuel cell [39] applications. BN-based materials possess excellent electrochemical properties, which makes them promising candidates for electrochemical applications such as SCs and electrochemical sensors [40]. In this review article, we have summarized recent progress in the design and preparation of BN-based electrodes for the development of SCs and electrochemical sensors. This review may benefit readers who are working on the fabrication of SCs and electrochemical sensors using BN-based materials.

2. BN-Based Electrode Materials for SCs

In previous years, various electrode materials have been explored for the development of SCs. BN-based materials have demonstrated good performance for the construction of electrode materials for SCs applications. BN has been combined with various materials such as reduced graphene oxide (rGO). It is expected that BN-based hybrid composites should demonstrate improved electrochemical performance for SCs. Thus, Gao et al. [41] reported the formation of BN/rGO composite by employing a liquid-phase exfoliation-assisted method. The synthesized BN/rGO was explored for its application in SCs and experimental findings revealed the presence of excellent electrochemical properties. The BN/rGO composite-based electrode showed a specific capacitance of 140 F/g at a current density of 2 A/g. The proposed electrode also showed cyclic stability for 1000 cycles. It is believed that the presence of synergism between BN and rGO enhanced the electrochemical activity of the proposed electrode for SCs. Saha et al. [42] reported the electrochemical

preparation of sulfanilic acid azochromotrop (SAA)-functionalized rGO/h-BN on a Ni foam-based electrode. The preparation of SAA@rGO/h-BN@Ni is demonstrated in Figure 1. The authors used scanning electron microscopy (SEM) and transmission electron microscopy (TEM) to study the morphological properties of the prepared materials. The electrochemical performance of the prepared SAA@rGO/h-BN@Ni was studied for application in SCs and an excellent capacitance of 1300 F/g was obtained using SAA@rGO/h-BN@Ni as electrode. The proposed SC electrode also retained excellent stability for 10,000 cycles.

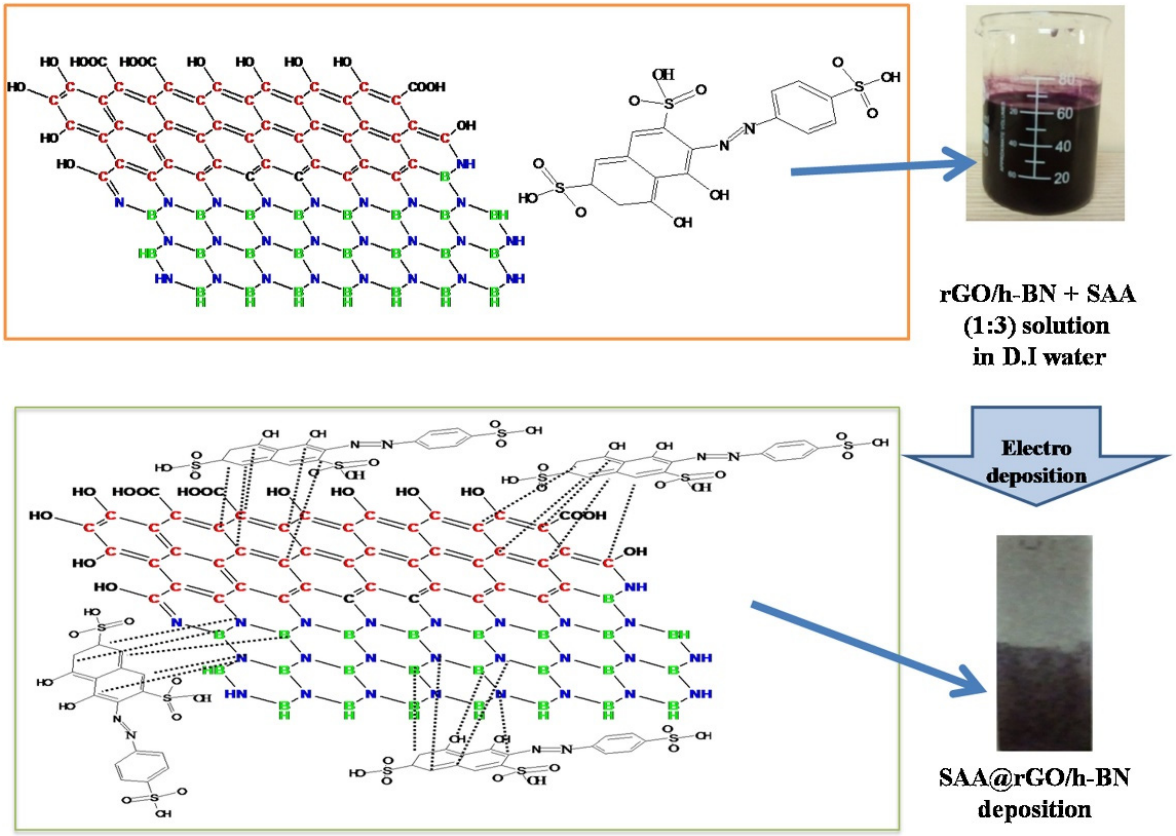

Figure 1. Schematic representation of the preparation of SAA@rGO/h-BN@Ni electrode. Reproduced with permission [42].

It is believed that the amount of rGO may play a significant role within the h-BN moiety and has the potential to reduce the electronic work function but increase the density of states (DOS) of the proposed electrodes. Saha et al. [43] also investigated the role of rGO on the surface of h-BN for SC applications. The h-BN with a rod-like structure was aligned as a sheet and combined with rGO. The prepared h-BN/rGO super-lattice was used as an SC material using cyclic voltammetry (CV) and charge–discharge (CD) as electrochemical techniques for the investigation of its capacitive properties. An excellent specific capacitance of 960 F/g was reported for the proposed h-BN/rGO super-lattice-based electrode with stability of 10,000 CD cycles. This suggested that h-BN/rGO-based electrodes are efficient for the construction of next-generation SCs. Patil et al. [44] reported a benign approach for the preparation of a 2D/3D heterostructure of h-BN/rGO using a ball milling-assisted method. The 2 wt% h-BN/rGO-based electrode showed a specific capacitance of 304 F/g at 1 A/g under alkaline conditions. In contrast, the 2 wt% h-BN/rGO-based electrode showed a specific capacitance of 226 F/g at 1 A/g under acidic conditions. This proposed electrode also demonstrates stability up to 10,000 cycles. It may be noted that the improved capacitance and stability may be ascribed to the non-hierarchical assembly of the 2D/3D structure, which may have provided an efficient interface for the

electro-active species. Lee et al. [45] proposed the preparation of a novel electrode material for SCs. The preparation of the proposed material is illustrated in Figure 2. The authors also stated that functionalization of BN may show improved electrochemical properties.

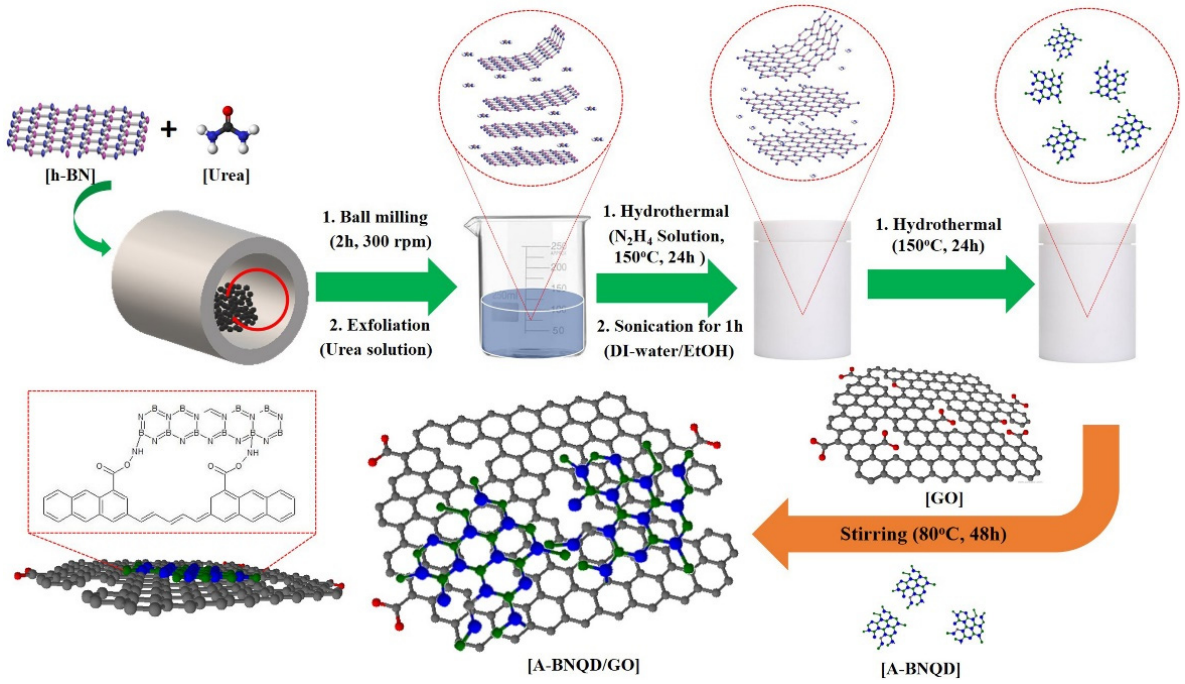

Figure 2. Schematic illustration for the synthesis of A-BNQD/GO. Reproduced with permission [45].

Thus, they prepared amine-functionalized BN quantum dots (A-BNQDs). The prepared A-BNQDs were further attached with rGO to form the A-BNQD/rGO composite. The A-BNQD/rGO composite exhibited higher catalytic activity compared to the raw BNQD/rGO or rGO. An improved capacitance of 90 F/g was observed at 1 A/g with good stability of 10,000 cycles. Rajendran et al. [46] reported the preparation of an h-BN-integrated rGO composite which demonstrated an excellent electrical conductivity of 5.36×10^4 S/m with a sheet resistance of 8.87 Ω/sq. The authors used simple strategies for the construction of a flexible paper-based electrode for SC applications. The fabricated electrode showed a specific capacitance of 321.95 F/g at 0.5 A/g. This prepared flexible electrode also showed excellent cyclic stability of 6000 CD cycles. Hassan et al. [47] anchored activated carbon (AC) nanospheres on BN nanoplates by using a benign pulsed-laser ablation in liquid approach. The authors used four different percentages (1%, 3%, 5%, and 10%) of BN in AC and the synthetic protocols are demonstrated in Figure 3a. The SEM images of the prepared samples are shown in Figure 3b–d. The surface morphological studies indicated that the electrode materials achieved efficient intercalation of AC nanospheres into BN nanoplates, which may have contributed to improving the SC performance of the proposed electrode. The authors used a gel polymer electrolyte (GPE) for the construction of the SCs. The authors investigated the electrochemical performance of the proposed electrodes using electrochemical impedance spectroscopy (EIS), CV, and GCD. The GCD curves of the different prepared electrodes (1% BN, 3% BN, 5% BN, and 10% BN in the AC electrode) at different current densities are shown in Figure 3e–h. It can be seen that all the prepared electrodes exhibited enhanced performance at 0.3 A/g. The overall GCD curves of all the electrodes (1% BN, 3% BN, 5% BN, and 10% BN in the AC electrode) at 0.3 A/g are summarized in Figure 3i. It is observed that 3% BN (BN3) has better performance compared to the other electrodes. The authors reported a specific capacitance of 348 F/g which is higher than that of BN1, BN5, and BN10.

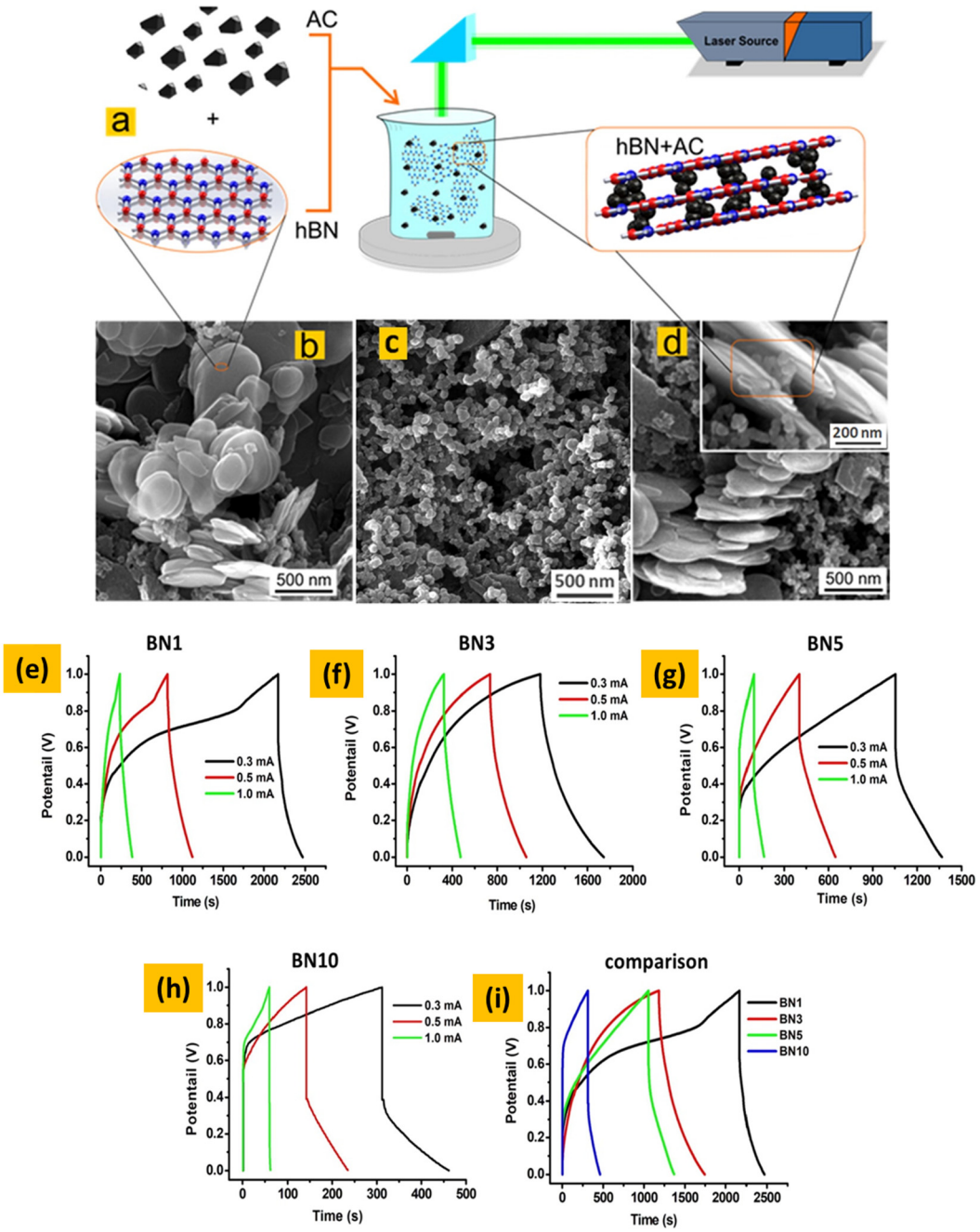

Figure 3. (**a**) Schematic diagram shows synthesis of h-BN and hBN + AC. SEM image of (**b**) BN, (**c**) pure AC, and (**d**) hBN + AC. Galvanostatic CD curves of (**e**) 1% BN, (**f**) 3% BN, (**g**) 5% BN, and (**h**) 10% BN in AC electrode. (**i**) Comparison of different electrodes at 0.3 A/g. Reproduced with permission [47].

Li et al. [48] explored AC as an anode material, with carbon-modified BN (h-BN/C) as the cathode material for application in an SC. The h-BN/C was prepared using a simple solid-state reaction. The electrochemical performance of the proposed electrode was checked by GCD. The GCD graphs of the h-BN/C- and h-BN-based electrodes at different current densities are shown in Figure 4b,c, respectively. It can be seen from Figure 4b that the h-BN/C-based electrode has higher capacitance at 0.5 A/g compared to the other current densities.

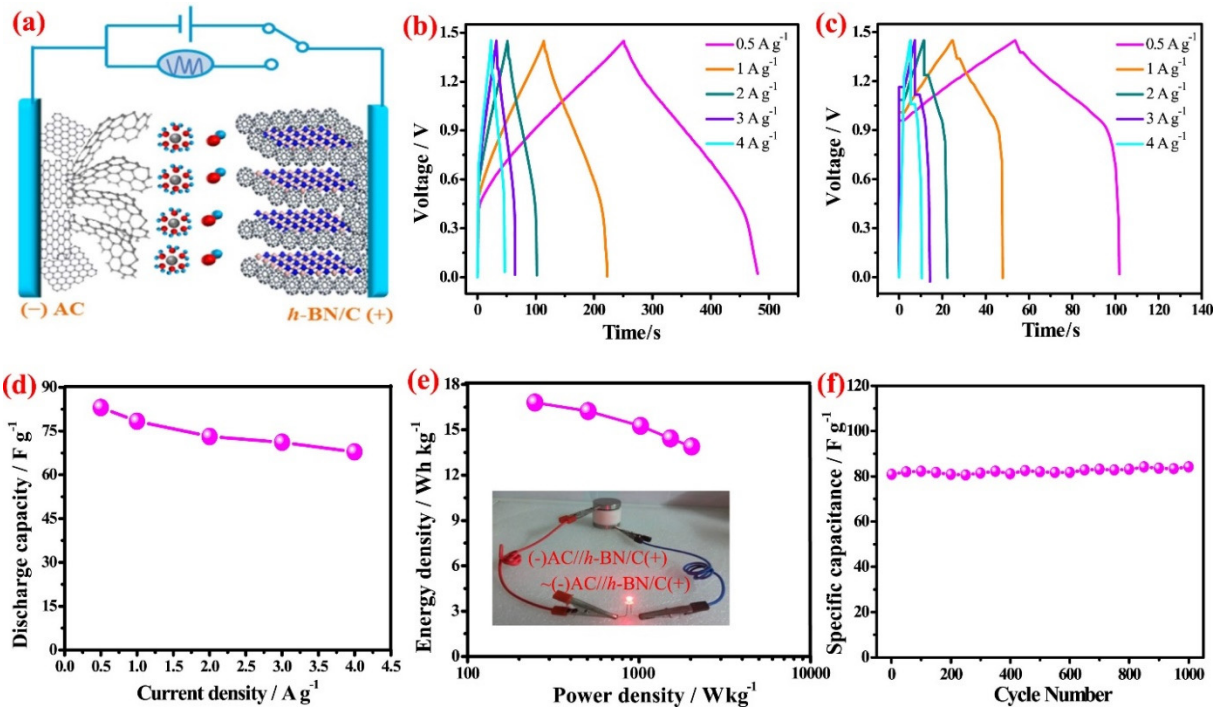

Figure 4. (**a**) Schematic of two-electrode testing system for SCs. GCD graphs of (**b**) h-BN/C and (**c**) h-BN-based electrodes. (**d**) Discharge capacitance versus current density curve of h-BN/C. (**e**) Ragone plots and inset shows LED indicator. (**f**) Cyclic stability results at 0.5 A/g. Reproduced with permission [48].

Similar patterns were observed for the h-BN-based electrode but the obtained capacitance was lower than for h-BN/C electrode-based SCs. An acceptable specific capacitance of 250 F/g was observed at a current density of 0.5 A/g. The discharge capacitance versus current density curve of h-BN/C is depicted in Figure 4d; it reveals that the electrode has higher electrochemical activity at 0.5 A/g. The Ragone plot shows the energy density versus power density graph in Figure 4e. The proposed electrode also demonstrated a good stability of 1000 cycles, as shown in Figure 4f. In other work, Gunday et al. [49] prepared polymer electrolytes consisting of a sulfonated polysulfone (SPSU) host polymer, with the ionic liquid (1-Ethyl-3-methyl-imidazolium tetrafluoroborate (IL)) used as the softening agent. hBN was adopted as the additive and the SCs were constructed under benign conditions.

The electrolyte and electrode preparations are described in Figure 5a. The electrochemical performance of the proposed SCs was checked by using GCD. The GCD curves of the SPSU/5% hBN/0.2 IL at different current densities are demonstrated in Figure 5b. The highest performance was observed at 1 A/g. Figure 5c shows the GCD cycles of SPSU/5% hBN/0.2 IL at 1 A/g. The specific capacitance of the SCs at 1 A/g are displayed in Figure 5d. The highest specific capacitance of 90.4 F/g was observed at 1 A/g. The authors also reported an interesting power density of 1100 W/kg and energy density of 43.8 Wh/kg. In a report by Barai et al. [50], a composite of α-MnO_2 nanorods (NRs) and BN nanoplatelets (BNNPs) for SC applications was described. The synthesis can be understood from the schematic illustration in Figure 6a. According to the plausible mechanism shown in Figure 6a, it was reported that initially H^+ was intercalated into the layer of BN. This may have expanded the BN layer and facilitated the intercalation of SO_4^- ions. The authors stated that it further facilitated the intercalation of K^+ and MnO_4^- into the layer of BN. It was also reported by the authors that the formation of α-MnO_2 in the BN may have hindered the re-stacking of BN sheets, forming BNNPs with a lower number of sheets. In

addition, evolution of the oxygen (O_2; during reaction) gas may have increased the pushing force and accelerated the exfoliation of the BN. The electrochemical performance of the α-MnO_2 NR/BNNP/CC and BNNP/CC electrodes were examined by obtaining their GCD curves in the potential window range of −0.3 V to 1.0 V. Figure 6b depicts the obtained GCD results and it is observed that α-MnO_2 NR/BNNP/CC had higher electrochemical performance and capacitance compared to the BNNP/CC. The observations show that α-MnO_2 NRs/BNNP/CC delivered a significant specific capacitance of 890 F/g at 0.41 A/g. The BNNPs demonstrated a lower specific capacitance of 1.30 F/g at 0.024 A/g. Figure 6c shows the specific capacitance versus current density curve of α-MnO_2 NRs/BNNP/CC. It can be seen that specific capacitance (F/g) decreases with increasing current density (A/g). A similar trend was observed for the BNNP/CC electrode, as displayed in the inset of Figure 6c. The authors found that the GCD results for α-MnO_2 NRs/BNNP/CC followed non-linear pseudocapacitive behavior and had a voltage plateau. It was confirmed by the authors that the GCD results were in good agreement with the CV results.

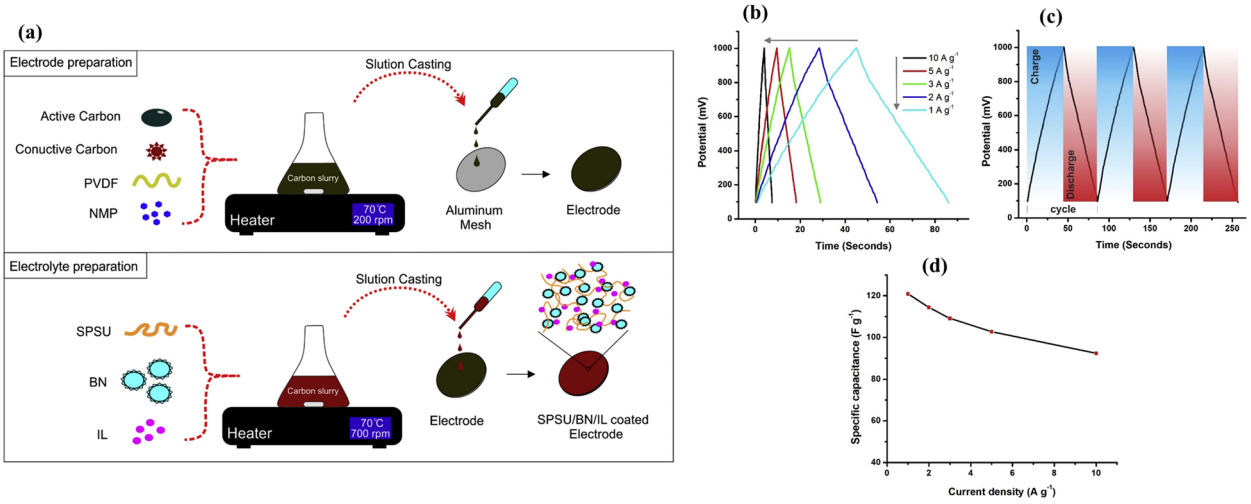

Figure 5. (**a**) Schematic graph shows the preparation of electrode and electrolyte preparation. (**b**) GCD curves of SPSU/5% hBN/0.2 IL. (**c**) GCD cycles of SPSU/5% hBN/0.2 IL at 1 A/g. (**d**) Specific capacitance of SPSU/5% hBN/0.2 IL. Reproduced with permission [49].

The Ragone plot of α-MnO_2 NRs/BNNP/CC shows the energy density–power density curve (Figure 6d). In contrast, the Ragone plot of BNNP/CC is placed in the inset of Figure 6d. It can be seen that the energy density decreases with increasing power density values. Furthermore, the authors studied the stability of the proposed electrode for SCs and the obtained results are provided in Figure 6e. The proposed electrode retained excellent capacitance and specific capacitance only decreased by 5.9% after 2000 cycles. This indicated the acceptable stability for 2000 cycles. The improved performance of the α-MnO_2 NRs/BNNP/CC may be ascribed to the presence of synergistic interactions, and the crystallinity and high conductivity of the α-MnO_2 NRs/BNNP/CC. The EIS results of the α-MnO_2 NRs/BNNP/CC and BNNP/CC are presented in Figure 6f (frequency = 1 Hz to 0.1 MHz). The authors found that a perfect semicircle was observed for α-MnO_2 NRs/BNNP/CC, whereas a depressed semicircle appeared for BNNP/CC. The Randles circuit model-based calculations for α-MnO_2 NRs/BNNP/CC showed the charge transfer resistance (Rct) and sheet resistance (Rs) values of 4.5 Ω and 0.5 Ω, respectively. In another case, BNNP/CC exhibited Rs and Rct values of 4.8 Ω and 49 Ω, respectively. This confirmed that α-MnO_2 NRs/BNNP/CC has higher electrical conductivity. The authors also used the EIS method before and after the GCD cycles and the obtained data are depicted in Figure 6g. The authors found that an Rs value of 0.52 Ω

and Rct value 5.2 Ω were observed for α-MnO_2 NRs/BNNP/CC after 2000 GCD cycles. This indicated the higher electrochemical stability of the above optimized electrode.

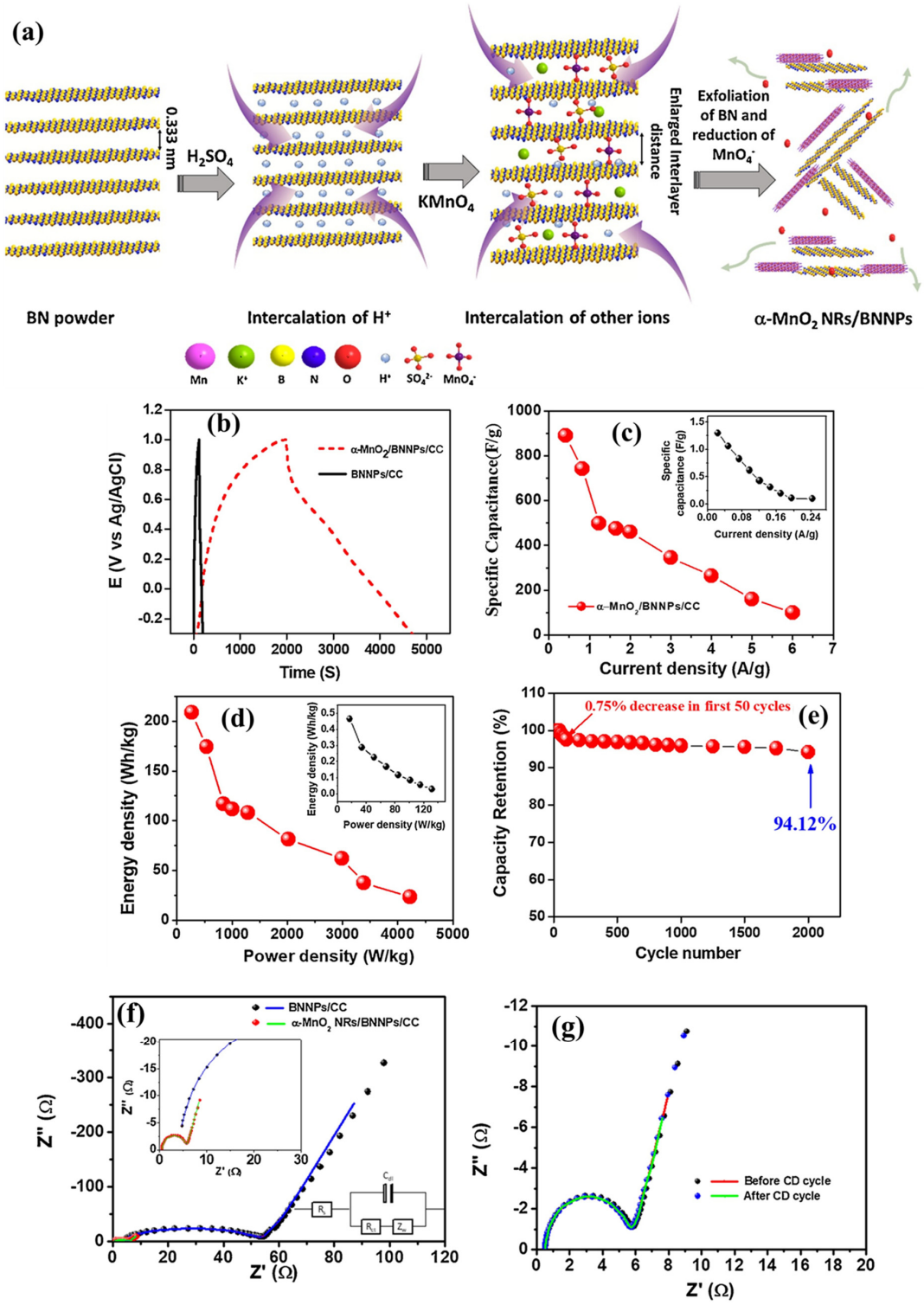

Figure 6. (**a**) Schematic graphs show synthesis of α-MnO_2 NRs/BNNPs. (**b**) GCD curves of α-MnO_2 NRs/BNNP/CC and BNNP/CC electrodes. (**c**) Specific capacitance versus current density curve of α-MnO_2 NRs/BNNP/CC (inset shows specific capacitance versus current density curve of BNNP/CC). (**d**) Ragone plot of α-MnO_2 NRs/BNNP/CC (inset: Ragone plot of BNNP/CC). (**e**) Stability of α-MnO_2 NRs/BNNP/CC. (**f**) Nyquist curves of α-MnO_2 NRs/BNNP/CC and BNNP/CC. Upper inset shows magnified region and lower inset shows circuit. (**g**) Nyquist curves of α-MnO_2 NRs/BNNP/CC before and after stability. Reproduced with permission [50].

Lin et al. [51] reported gauze-like h-BN nanosheets (NSs) doped onto the surface of β-MnO_2 nanobelts (NBs) by utilizing a benign one-step hydrothermal technique. The authors found that the agglomeration behavior of β-MnO_2 NBs was inhibited by the presence of h-BN. Moreover, the prepared composite itself built a 3D structure, which is expected to enhance the capacitive activity of the fabricated electrode for SCs. The authors reported that the h-BN/β-MnO_2 composite demonstrated a specific capacitance of 578.4 F/g at 0.5 mA/cm^2 (0.36 A/g) and retained 97.1% capacitance of compared to the initial performance after 5000 cycles. Maity et al. [52] proposed a novel electrode material for SC application. The authors synthesized zinc cobalt sulfide (ZCS) with various materials to enhance the capacitive performance of the SCs. In this connection, ZCS, ZCS/BN, ZCS/CNT, ZCS/BN/CNT, and ZCS/BN/CNT/PPY were synthesized using a hydrothermal-assisted method, as shown in Figure 7.

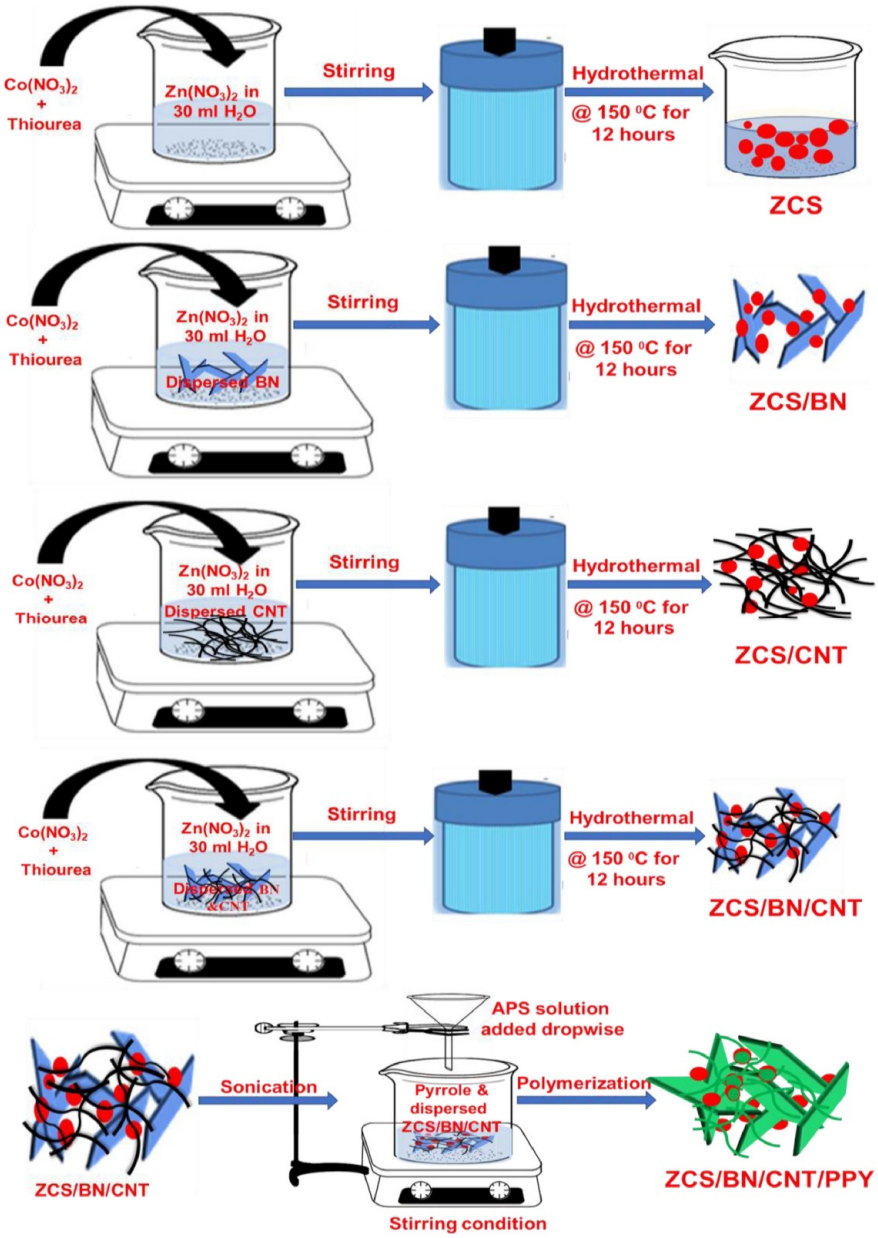

Figure 7. Schematic of synthetic protocols for the preparation of ZCS, ZCS/BN, ZCS/CNT, ZCS/BN/CNT, and ZCS/BN/CNT/PPY. Reproduced with permission [52].

The formation of the synthesized ZCS, ZCS/BN, ZCS/CNT, ZCS/BN/CNT, and ZCS/BN/CNT/PPY was confirmed by the XRD technique. The presence of ZCS-, BN-, and PPY-coated CNT was authenticated by TEM. The TEM results are shown in Figure 8a,b.

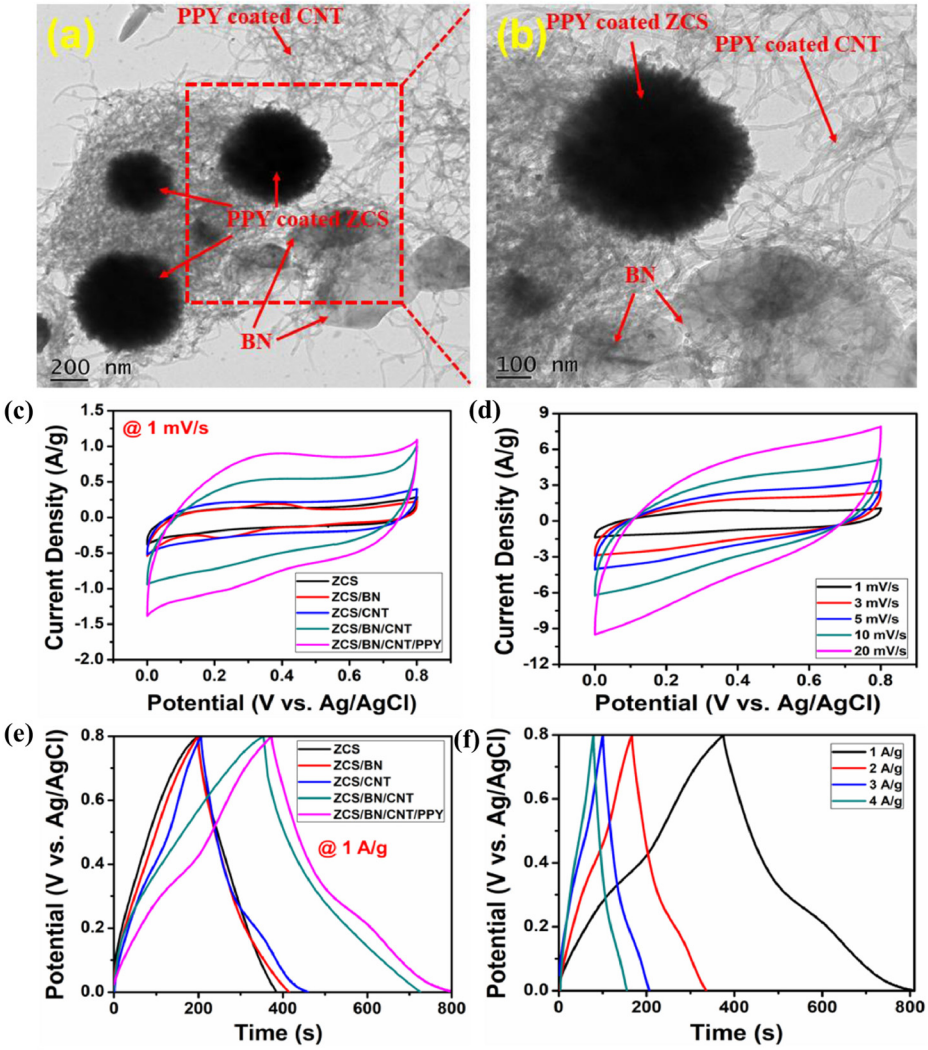

Figure 8. (**a**,**b**) TEM images of ZCS/BN/CNT/PPY at different magnifications. (**c**) CV curves of ZCS, ZCS/BN, ZCS/CNT, ZCS/BN/CNT, and ZCS/BN/CNT/PPY. (**d**) CVs of the ZCS/BN/CNT/PPY at various applied scan rates. (**e**) GCD graphs of the ZCS, ZCS/BN, ZCS/CNT, ZCS/BN/CNT, and ZCS/BN/CNT/PPY at 1 A/g. (**f**) GCD plots of ZCS/BN/CNT/PPY at various current densities. Reproduced with permission [52].

The TEM results suggested that the spheres were composed of a large number of rough nanocrystals. It was stated that a self-assembly mechanism may benefit the growth of the sphere-shaped structures with rough surfaces (Figure 8a). It was seen that PPY-modified CNT was grown on the BN sheets and ZCS spheres were wrapped by PPY-modified CNTs. These structures may be beneficial for electrochemical reactions. Furthermore, the authors studied the electrochemical performance of the ZCS, ZCS/BN, ZCS/CNT, ZCS/BN/CNT, and ZCS/BN/CNT/PPY electrodes using CV and the obtained results are displayed in Figure 8c. It was found that ZCS/BN/CNT/PPY had higher electrochemical activity compared to the other electrodes. Furthermore, CVs of the ZCS/BN/CNT/PPY were obtained at various scan rates, as shown in Figure 8d. The authors further obtained GCD curves of the GCD graphs of the ZCS, ZCS/BN, ZCS/CNT, ZCS/BN/CNT, and ZCS/BN/CNT/PPY and found that ZCS/BN/CNT/PPY had a higher capacitive performance compared to the other materials, as demonstrated in Figure 8e. The GCD graphs

of the ZCS/BN/CNT/PPY at different current densities are displayed in Figure 8f. The authors found that ZCS/BN/CNT/PPY demonstrated higher capacitance at 1 A/g. The authors also reported excellent cyclic stability of 10,000 cycles.

Panicker et al. [53] prepared electrode material using simple synthetic protocols. In this connection, the authors prepared an h-BN/rGO/CdS composite using a hydrothermal method (Figure 9a). Furthermore, the authors synthesized h-BN/rGO/CdS@PPy using a chemical oxidative polymerization approach, as depicted in Figure 9b. The synthesized materials were applied as the electrode material for SCs. The electrochemical investigations showed that rGO/CdS had a charge transfer resistance (Rct) value of 2.90 Ω, whereas h-BN/rGO/CdS had an Rct of 1.70 Ω. In the case of h-BN/rGO/CdS@PPy, the lowest Rct of 0.92 Ω was observed. This suggested that h-BN/rGO/CdS@PPy had excellent conductive properties compared to the other electrodes. The GCD results of the prepared electrodes suggested that h-BN/rGO/CdS@PPy had a high specific capacitance of 1435 F/g at 1 A/g. The authors also reported excellent cyclic stability of 5000 cycles for h-BN/rGO/CdS@PPy-based SCs.

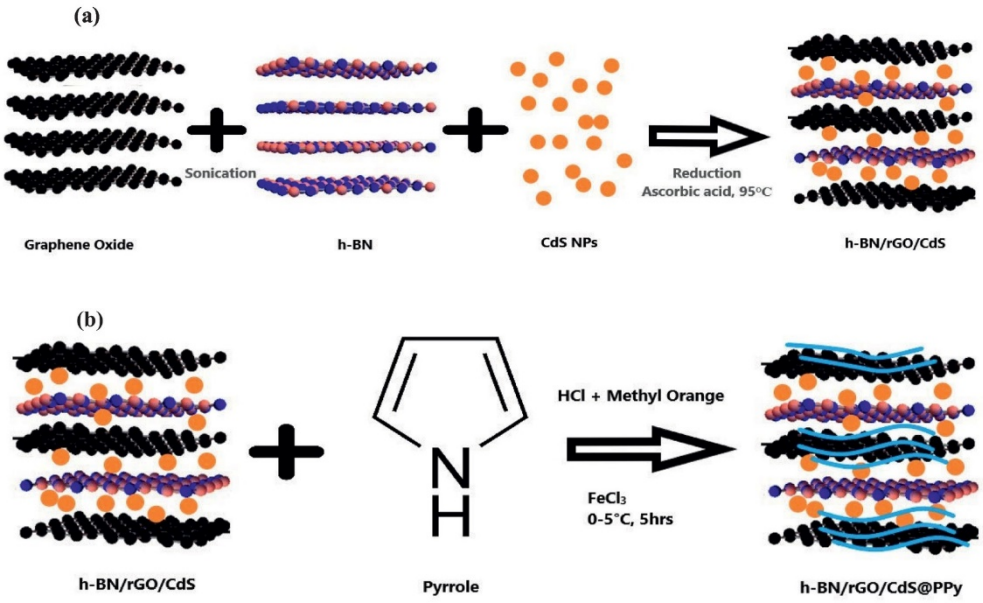

Figure 9. Schematic picture shows the preparation of h-BN/rGO/CdS nanocomposite (**a**) and h-BN/rGO/CdS@PPy (**b**). Reproduced with permission [53].

Maity et al. [54] also proposed an efficient electrode material for SC applications. The authors prepared functionalized BN (m_K-BN) and CNT stabilized with CuO using a hydrothermal method. The authors proposed that incorporation of CNT may improve the charge storage properties of the fabricated electrode for SCs. The synthesized CuO/m_K-BN/CNT composite showed a specific capacitance of 425 F/g. The proposed electrode material also exhibited excellent cyclic stability of 10,000 cycles. Sakaray et al. [55] reported the preparation of a novel electrode material for the construction of SCs. The ternary composite of PANI/MoO_3/h-BN was synthesized and characterized by the XRD and SEM methods. Furthermore, PANI/MoO_3/h-BN was explored for SC application and electrochemical studies revealed that the PANI/MoO_3/h-BN-based electrode exhibited a specific capacitance of 518 F/g. Maity et al. [56] reported a novel approach for the preparation of Zn-MoS_2/CDs@BN using cigarette smoke as the carbon source for the preparation of CDs. The synthetic process for the preparation of CDs, CDs@BN, and Zn-MoS_2/CDs@BN are described in Figure 10. The authors found that specific capacitances of 173 F/g, 252 F/g, 315 F/g, and 397 F/g were observed for MoS_2, Zn-MoS_2, MoS_2/CDs@BN, and Zn-MoS_2/CDs@BN-based SCs, respectively. This confirmed that Zn-MoS_2/CDs@BN

has excellent electrochemical properties and the presence of synergism enhanced the specific capacitance.

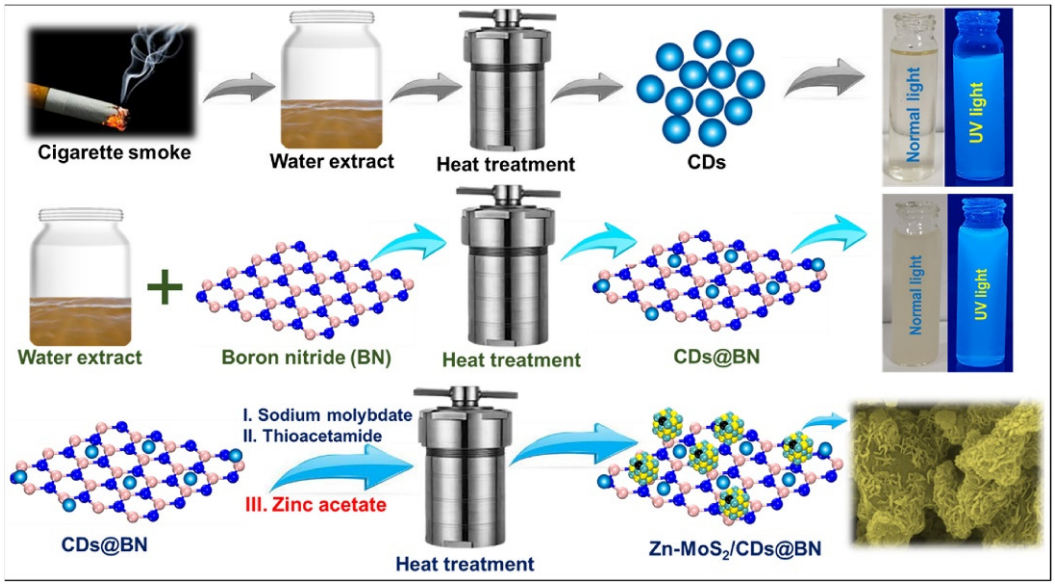

Figure 10. Schematic graph showing synthesis of Zn-MoS_2/CDs@BN. Reproduced with permission [56].

In a report by Rahman et al. [57], a conducting polymer polyaniline (PANI)-based composite was synthesized with h-BN and PPy. The PANI/h-BN and PANI-PPy/h-BN were synthesized in well-organized conditions and characterized under systematic conditions. The formation of the PANI/h-BN and PANI-PPy/h-BN were authenticated by XRD and SEM. The authors used the GCD method to examine the electrochemical performance of the PANI, PANI/h-BN, and PANI-PPy/h-BN for SC applications. The authors reported a specific capacitance of 451, 927, and 615 F/g for PANI, PANI/h-BN, and PANI-PPy/h-BN composite-based SCs at 10 mV/s, respectively. In a recent work, Zhao et al. [58] reported a hydrothermal ball milling synthesis method for the preparation of hBN-incorporated cobalt molybdate ($CoMoO_4$). The physicochemical properties of the synthesized $CoMoO_4$@hBN composite were studied by XRD, SEM, and XPS. The synthesized $CoMoO_4$@hBN composite was used as an electrode material for SCs and the obtained results demonstrated an excellent specific capacitance of 1682.7 F/g at 1 A/g. The pristine $CoMoO_4$ exhibited a specific capacitance of 1228.4 F/g at 1 A/g, which is lower than that of the $CoMoO_4$@hBN composite. This indicated that the presence of synergism between $CoMoO_4$ and hBN improved the capacitance of the $CoMoO_4$@hBN composite-based SCs. Dhamodharan K et al. [59] reported ultrasonic-assisted hydrothermal synthesis of exfoliated hBN NSs decorated with MoS_2 NFs. The prepared electrode material was characterized by SEM, which demonstrated that MoS_2 consists of flower-shaped structures, whereas hBN has a sheet-like structure. The hBN/MoS_2 composite showed a specific capacitance of 411.5 C/g at 10 mV/s. In another report, Sharma et al. [60] fabricated a 2D-hBN-modified electrode for electrochemical applications. The 2D-hBN was prepared using a hydrothermal approach and the 2D-hBN-modified electrode was used as the working electrode and the authors obtained a specific capacitance of 83 F/g at 2 mV/s. The proposed electrode also retained good capacitance up to 2000 cycles. The electrochemical super-capacitive performance of the BN-based composite materials are displayed in Table 1.

Table 1. Capacitance and other parameters of the BN-based composites for SCs.

Electrode/Material	Electrolyte	Stability Cycles	Specific Capacitance (F/g)	Current Density (A/g)	Refs.
BN/rGO	6 M KOH	1000	140	2	[41]
SAA@GBN2@Ni	6 M KOH	10,000	1300	3	[42]
h-BN/rGO	6 M KOH	10,000	960	1	[43]
h-BN/rGO	Alkaline (pH 13)	20,000	304	1	[44]
A-BNQD/rGO	2 M KOH	10,000	256.8	1	[45]
BN3	PAMPS	5000	348	0.3	[47]
h-BN/C	2 M KOH	1000	250	0.5	[48]
α-MnO_2 NRs/BNNP/CC	-	2000	890	0.41	[50]
h-BN/β-MnO_2	-	5000	578.4	0.36	[51]
ZCS/BN/CNT/PPY	1 M KCl	10,000	785	1	[52]
h-BN/rGO/CdS@PPy	3 M KOH	5000	1435	1	[53]
PMB-135	6 M KOH	-	518	1	[55]
Zn–MoS_2/CDs@BN	3 M KOH	10,000	397	1	[56]
PANI-PPy/h-BN	1 M Na_2SO_4	100	615	10 mV/s	[57]
$CoMoO_4$@hBN	6 M KOH	5000	1682.7	1	[58]
Exfoliated h-BN-MoS_2	3 M KOH	4000	411.5 C/g	10 mV/s	[59]
hBN	2 M KOH	2000	83	2 mV/s	[60]

3. BN-Based Electrode Materials for Electrochemical Sensing Applications

In recent years, a large number of BN-based electrochemical sensors have been developed and their performances reported. In this section, we have summarized the recently published electrochemical sensors using BN-based electrode materials. In this connection, Zhang et al. [61] reported the hydrothermal synthesis of Cu-h-BNNs for electrochemical sensing of nitrite. The prepared material was coated on a glassy carbon electrode, i.e., GCE, and its performance was checked by using EIS, CV, and differential pulse voltammetry, i.e., DPV. The electrochemical studies showed that the Cu-h-BNNs/GCE exhibited a limit of detection, i.e., LOD of 0.03 μM and linear range of 0.09 μM to 9853.45 μM. The authors also reported acceptable real-sample performance of the proposed electrode in river water samples and good selectivity towards the sensing of nitrite. Square wave voltammetry, i.e., SWV, is one of the more sensitive techniques for the detection of various analytes. In this connection, Fu et al. [62] reported the facile synthesis of Au NP-loaded BN for the determination of flavonoid luteolin in peanut hulls and Perilla samples. The authors prepared BNNS-Au NPs using a microwave-assisted method and the synthesized sample was deposited on the surface of GCE. The sensing ability of the BNNS-Au NPs/GCE was evaluated by exploring CV and SWV. The authors also optimized the pH of the sensing system and reported an LOD of 1.7 pM with a linear range of 5 to 1200 pM and 0.02 to 10 μM. The BNNS-Au NPs/GCE also showed good stability and acceptable selectivity. Yola et al. [63] reported the fabrication of a serotonin (SER) neurotransmitter using the CV and DPV techniques. The prepared composite material of graphene quantum dots and 2D hBN (GQDs/2D-hBN) was coated on the surface of GCE and its electrochemical ability was checked by employing EIS. The electrode preparation and working is illustrated in Figure 11. The constructed GQDs/2D-hBN/GCE exhibited an LOD of 2×10^{-13} M and a

linear range of 1.0×10^{-12} to 1.0×10^{-8} M. The authors also reported good performance of the GQDs/2D-hBN/GCE for the sensing of the target in a urine sample.

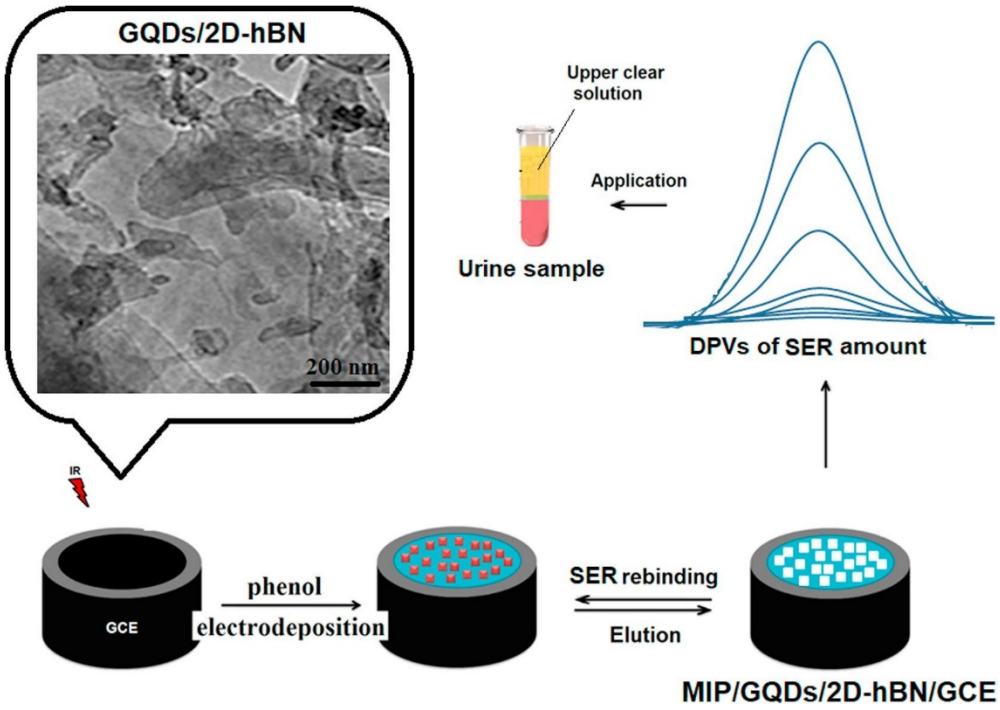

Figure 11. Schematic illustration of the fabrication and working of MIP/GQDs/2D-hBN/GCE. Reproduced with permission [63].

In other work, Yola et al. [64] reported the electrochemical sensing of β-agonists (phenylethanolamine A; PEA, clenbuterol; CLE, ractopamine; RAC, and salbutamol; SAL) using CV and DPV methods. A new electrode material of 2D-hBN and f-MWCNTs was prepared using simple synthetic protocols and characterized by the XRD and SEM techniques. Furthermore, the synthesized 2D-hBN/f-MWCNTs composite was deposited on GCE and its electro-catalytic properties were studied by employing CV and EIS. Furthermore, the sensing activity of the 2D-hBN/f-MWCNT-coated GCE was determined by the DPV technique. The fabricated sensor demonstrated an LOD of 1.0×10^{-13} for the sensing of PEA, CLE, RAC, and SAL. A linear range of 1.0×10^{-12} to 1.0×10^{-8} M was also reported for the determination of PEA, CLE, RAC, and SAL. The proposed sensor was also found to be stable, repeatable, and selective for the sensing of β-agonists. Hatamluyi et al. [65] reported the fabrication of a carbon quantum dots (CQDs@HBNNS/UiO-66-NH_2/MIP/GCE) material for selective sensing of Oxaliplatin (OXA). The authors reported that the improved electrochemical performance and sensitivity of the proposed MIP sensor (CQDs@HBNNS/UiO-66-NH_2/MIP/GCE) was due to the incorporation of UiO-66-NH_2, which provided a highly porous structure and binding sites with high specific surface area. In addition, CQDs@HBNNS-NCs have excellent electrical conductivity and the presence of synergistic effects may have promoted efficient electron transfer. Thus, the authors reported an excellent LOD of 0.37 nM in aqueous solution and 0.40 nM in a pharmaceutical sample. LODs of 0.39 nM and 0.41 nM were found in blood serum and urine samples, respectively. Karimi-Maleh et al. [66] proposed the construction of a composite of Pt NPs/polyoxometalate(POM)/2D-hBN and 1-hexyl-3-methylimidazolium chloride (HMICl) for the sensing of N-hydroxysuccinimide. The sensing performance of the reported sensor was evaluated by using CV and chronoamperometry methods. The constructed sensor (HMICl-PtNPs/POM/2D-hBN/POMBNS/CPE) demonstrated an LOD of 60 nM with a linear range of 0.1 to 300 μM. Shen et al. [67] synthesized defect-rich hexagonal BN (D-h-BN)

using a one-step calcination route via a single source precursor. The synthesized D-h-BN was coated on GCE and its electrochemical activity was checked by employing the CV and DPV techniques. Furthermore, sensing of 4-aminophenol (4-AP) and phenol (Ph) were carried out using the above mentioned electrode. The D-h-BN--coated GCE demonstrated good LODs of 0.003 and 0.035 μM for the determination of 4-AP and Ph, respectively. The proposed sensor also demonstrated decent selectivity, reproducibility, and a linear range of 0.1 to 30 μM. The authors also reported excellent real-sample recoveries in lake and tap water samples. Renganathan et al. [68] proposed a benign strategy for the preparation of Pd NPs on BN and characterized their formation by XPS. The synthesized Pd NPs/BN was deposited on GCE and its electrochemical activity was evaluated for the sensing of the fatal organophosphorus pesticide paraoxon ethyl (PXL). The authors adopted the CV and LSV methods for the determination of the target analytes and found that the proposed electrode exhibited good electro-catalytic properties for the determination of PXL. The presence of synergism, a larger surface area, and improved electrical conductivity of the prepared electrode demonstrated acceptable selectivity and an LOD of 0.003 μM with a linear range of 0.01 to 210 μM towards the detection of PXL. The constructed electrode also showed excellent recoveries in river samples for the monitoring of PXL. Kokulnathan et al. [69] reported the fabrication of an efficient electrode modifier for the sensing of furazolidone. The authors reported the synthesis of a BN/halloysite-nanotube (h-BN/HNTs) composite using ultra-sonication-assisted synthetic protocols, as shown in Figure 12. The synthesized h-BN/HNTs was coated on GCE and its CV responses were recorded for the sensing of furazolidone. The proposed electrode showed better electrochemical activity compared to the bare GCE, HNTs/GCE, or h-BN/GCE electrodes for 200 μM furazolidone. The constructed electrode showed an LOD of 0.001 μM with a linear range of 0.009 to 173 μM furazolidone. The sensing mechanism can be seen in Figure 12. The authors also found that the constructed electrode had good selectivity and real-sample performance in egg and milk samples.

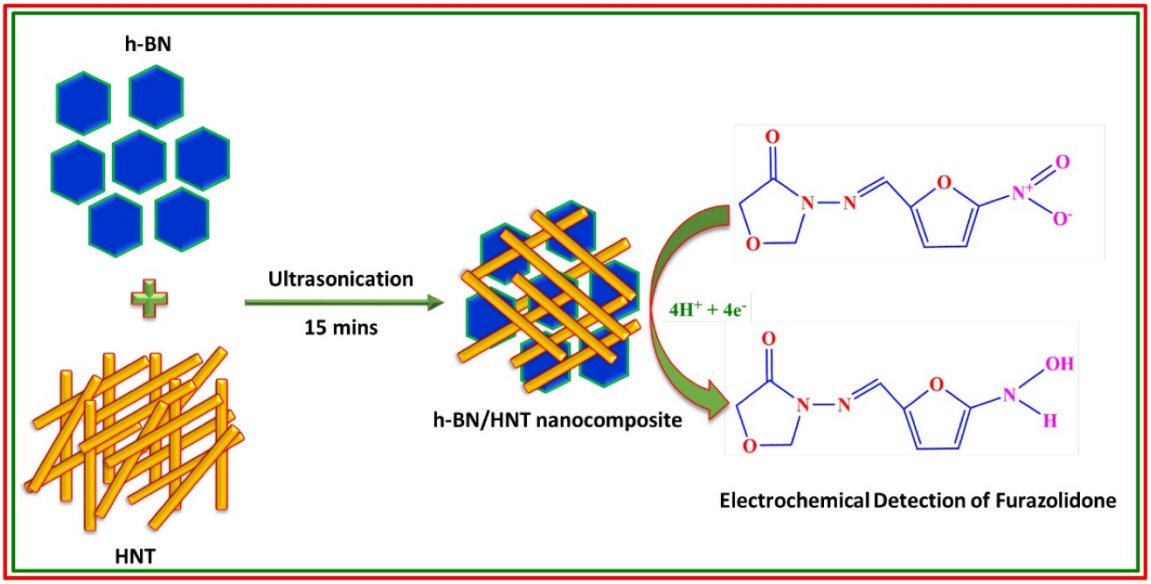

Figure 12. Schematic graph shows the preparation of h-BN/HNT composite and probable mechanism for the sensing of furazolidone. Reproduced with permission [69].

It is well understood that selective detection of nicotine in biological and biomedical samples is of great significance to screen patients affected by the neurodegenerative diseases which may occur due to tobacco addiction. In this regard, Jerome et al. [70] reported a scalable top-down method for the preparation of BN-doped graphene (BN/graphene)

film. The prepared BN/graphene was characterized by Fourier transform infrared (FTIR), UV–visible (UV–vis), and XPS. The authors found that the prepared BN/graphene had good electrical conductivity, as suggested by EIS studies. The prepared material was applied as a nicotine sensor and reported a good LOD of 0.42 μM with a linear range of 1 to 1000 μM. The authors also reported excellent selectivity for nicotine sensing in the presence of various interfering species such as paracetamol, dopamine, glucose, melamine, uric acid, and cysteine. The prepared sensor also had good reproducibility and selectivity and real-sample recoveries in tobacco samples. Flutamide (FLT) is one of the non-steroidal anti-androgen drugs which is used for the treatment of prostate cancer. Unfortunately, overdoses of FLT can be responsible for severe side effects. Thus, it is essential to monitor the level of FLT and development of an efficient sensor is required for the selective and sensitive determination of FLT. Kesavan et al. [71] reported a co-precipitation method for the formation of an Mn_2O_3@h-BN composite. The schematic graph shows the synthesis of the Mn_2O_3@h-BN composite for FLT sensing in Figure 13a. This prepared material was deposited on a GCE surface and its electro-catalytic activity for the determination of FLT was studied by employing the CV and DPV. The CV results showed that Mn_2O_3@h-BN-modified GCE had better electrochemical performance compared to the bare GCE, h-BN-, or Mn_2O_3-modified GCE. This enhanced activity may be ascribed to the synergism and electrical conductivity, as suggested by the EIS studies. The CVs of the Mn_2O_3@h-BN for different amounts of FLT are shown in Figure 13b. The current response was linearly increased with increase in the concentration of FLT, as shown in Figure 13c. The obtained CVs of the Mn_2O_3@h-BN for 200 μM FLT at various scan rates are shown in Figure 13d and the observations showed that the current response linearly increased with increase in the scan rate (Figure 13e). The authors also investigated the effects of various pHs on the performance of the Mn_2O_3@h-BN-modified GCE for 200 μM FLT at various pHs (Figure 13f). The observations suggested that the prepared electrode had higher electrochemical activity at a pH of 7.0, as shown in Figure 13g. The authors achieved a good LOD of 0.0085 μM with a linear range of 0.08 to 1940 μM using DPV. This study also stated that fabricated sensor has acceptable selectivity towards the detection of FLT in the presence of glucose, Mg^{2+}, creatinine, ascorbic acid, caffeine, Cd^{2+}, uric acid, and Ca^{2+}.

Öndeş et al. [72] reported the fabrication of a cancer antigen 125 (CA125) sensor by preparing BNN-modified electrochemical immunosensors. The BNN-modified SPE exhibited an LOD of 1.18 U/mL with a linear range of 5 to 100 U/mL, with a stability of 45 days. Kesavan et al. [73] found that the combination of bimetallic NPs with 2D hBN may significantly enhance the electrical and electrochemical properties of the resulting composite electrode materials. In this regard, the authors synthesized iron vanadate nanoparticles ($FeVO_4$ NPs) supported on hBN to form FeV NPs/hBN as shown in Figure 14.

The synthesized material was deposited on SPCE and its electrochemical activity was determined for the detection of chlorpromazine (CPZ). The FeV NPs/30 hBN-modified SPCE demonstrated an excellent LOD of 0.004 μM and linear range of 0.04 to 2222.1 μM. The authors also demonstrated the presence of excellent selectivity, stability, and reproducibility for the sensing of CPZ. The proposed sensor also showed good real-sample recoveries in serum samples. Jeena N. Baby et al. [74] reported the synthesis of a strontium pyrophosphate-based composite with h-BN (SrP/h-BN) for electrochemical sensing studies. The synthesized SrP/h-BN composite was explored for the sensing of dopamine, and the electrochemical investigations revealed that an improved LOD of 0.3 μM was observed towards the detection of dopamine. The authors also reported a wide dynamic linear range of 1 nm to 150 μM and 170 μM to 337 μM. The SrP/h-BN-based sensor also demonstrated an impressive sensitivity of 19.6 ± 0.015 μA/μM.cm^2, with excellent recoveries in a human urine sample. It is of great significance to monitor the presence of organic pollutants in

the environment to avoid their negative impacts on the environment and aquatic life, as well as human beings. In 2022, Harikrishnan et al. [75] reported the construction of hydroquinone using CV, DPV, and amperometry methods. The authors synthesized a carbon nitride-modified BN (g-C_3N_4/BN) composite using a solvothermal method. The prepared g-C_3N_4/BN was explored as a catalyst/electrode modifier for the sensing of hydroquinone. The obtained results demonstrated that a good LOD of 8.2 nM was achieved towards the monitoring of hydroquinone using a g-C_3N_4/BN composite-based GC electrode. The authors also found that the proposed sensor had good performance for real-sample recovery in industrial waste water and tap water. Kokulnathan et al. [76] reported the fabrication of a flutamide (FTM) sensor using an h-BN-decorated bismuth oxide (Bi_2O_3/h-BN) composite as an electrode modifier. The synthesized Bi_2O_3/h-BN was coated on SPCE and explored as an FTM sensor. Electrochemical studies showed that the fabricated sensor was highly sensitive for the sensing of FTM, with an LOD of 9 nM. The FTM sensor also exhibits linear range of 0.04 to 87 μM, with a good response time. This interesting performance of the FTM sensor may be due to the existance of synergism between BN and Bi_2O_3 and various active sites, which may have provided better and efficient charge transfer. In another report, Kokulnathan et al. [77] also explored the construction of an electrochemical sensor by decorating BN with yttrium oxide (YO). The YO-decorated BN (YO/BN) composite was prepared by a benign sonochemical method. The authors found that the YO/BN-based electrode exhibited better electrochemical activity compared to YO- or BN-based electrodes. The YO/BN-based electrode was further used as a dopamine sensor, showing an LOD of 0.0003 μM with a linear range of 0.008 to 241 μM including sensitivity of 1.09 μA/μM.cm^2. The authors also achieved excellent selectivity, acceptable reproducibility, recovery, and stability for the monitoring of dopamine. Bhuvaneswari et al. [78] reported simple and efficient approaches for the construction of a flutamide (FLA) electrochemical sensor by employing a ternary composite by adopting the solvothermal method. The authors synthesized an rGO-wrapped bismuth vanadate ($BiVO_4$)-loaded chemically exfoliated boron nitride (CE-BN)-based ternary composite (Figure 15a). The synthesized $BiVO_4$-rGO/CE-BN composite was further used as an electro-catalyst for the monitoring of the FLA drug using the CV and DPV approaches. It was stated that the $BiVO_4$-rGO/CE-BN-coated GC electrode had higher catalytic activity for 150 μM FLA compared to the bare GC, rGO/GC, $BiVO_4$/GC, $BiVO_4$-rGO/GC, or CE-BN/GC electrodes using the CV technique.

The DPV results of the $BiVO_4$-rGO/CE-BN-coated GC electrode at various concentration of FLA are displayed in Figure 15b, whereas the corresponding linear calibration graphs are depicted in Figure 15c. It can be observe that the electro-catalytic peak current response increased with increases in the concentration of FLA. The proposed senor demonstrated an LOD of 0.011 μM with a sensitivity of 3.8028 μA/μM.cm^2 which also include linear range of 0.04 μM to 102.2 μM towards the monitoring of FLA. Furthermore, the authors studied the selective nature of the proposed sensor in the presence of various electro-active and interfering species, as shown in Figure 15d,e. It can be seen that the proposed sensor has excellent selectivity for the detection of FLA. This sensor was also used for real-sample investigations and the authors found acceptable/satisfactory recoveries in lake water samples. Öndeș et al. [79] used enzyme-modified BNNs as a 2D electrode material for the sensing of uric acid. The enzyme-modified-BNN-based electrode shows LOD of 0.14 μM and sensitivity of 0.5248 μA/μM.cm^2. The authors also found that the enzyme-modified-BNN-based electrode could be used for the determination for uric acid with a wide linear range of 5 to 3000 μM and good reproducibility, selectivity, and reusability. A human serum sample was also used to further check its practical applicability and the authors achieved satisfactory results. Nitrofurazone (NF) is one of the antibiotics which is extensively used in clinical treatments, but its uncontrolled use or disposal wastage may

cause serious issues to the ecosystem and have negative impacts on the environment. Thus, Thirumalraj et al. [80] explored a novel electrode material for the monitoring of NF using tin selenide (SnSe)-integrated h-BN as an electrode modifier. The prepared electrode modifier (SnSe/h-BN) was deposited onto the active area of the GCE and electrochemical methods were adopted for the sensing of NF. The SnSe/h-BN-modified electrode also showed good performance compared to the h-BN/GCE and SnSe/GCE. The authors achieved an LOD of 0.34 nM with a sensitivity of 1.927 μA/μM.cm^2. The proposed sensor exhibited a dual linear range of 0.001 μM to 12.12 μM and 15.2 μM to 342.2 μM. This enhanced performance of the SnSe/h-BN-based electrode may be ascribed to the larger surface area and synergistic interaction between the SnSe and h-BN, which may have improved the kinetics of the electron transfer over the interface of the working electrode and electrolyte. This sensor also demonstrated satisfactory results for real samples studied in water and urine samples. Habibi et al. [81] a synthesized copper/zeolitic imidazolate framework-8-integrated BN (Cu/ZIF-8/BN) composite, which was further coated onto the surface of a GC electrode. The Cu/ZIF-8/BN-coated GCE was explored as a clopidogrel (CPG) sensor by utilizing the CV and amperometric sensing methods. The Cu/ZIF-8/BN-coated GCE showed an LOD of 3.5 μM with linear ranges of 5 μM to 39 μM and 39 μM to 107 μM for the efficient determination of CPG. The authors also reported excellent recovery of real-sample investigations in blood serum and pharmaceutical samples, which suggested its practical ability for commercialization. Jeyaraman et al. [82] proposed that the crystal phase may affect the electrochemical properties of working electrodes. The authors also stated that mixed phases of metal ions with different oxidation states may improve electrochemical activity by enabling conductivity. Additionally, 2D materials improve the adsorption of sensing analytes owing to their high surface area and properties. Thus, the authors prepared a mixed spinel metal oxide [Co, Mn oxides (CMO NPs)]/f-BN composite, as shown in Figure 16. The synthesized material was denoted as CMO NPs/f-BN and its electrochemical activity was evaluated for the sensing of the herbicide diuron. The obtained results demonstrated an LOD of 13 nM with linear ranges of 0.01 μM to 419 μM and 569 μM to 1770 μM. The fabricated sensor also demonstrated a sensitivity of 0.323 μA μM.cm^2 with good selectivity, stability, and repeatability/reproducibility. The acceptable recoveries in real-sample studies also demonstrated its potential for practical applications.

In another report, Bhuvaneswari et al. [83] proposed that shaped influenced NPs across the working electrodes (such as GCE) may promote the electrochemical activities. In this context, the authors synthesized calcium tungstate, cobalt tungstate, lead tungstate, copper tungstate, and barium tungstate (Ca(WO_4), CaW; Co(WO_4), CoW; Pb(WO_4), PbW; Cu(WO_4), CuW; and Ba(WO_4), BaW) on CE-BN. The synthesis of the different materials (CaW, BaW, CoW, PbW, and CuW) mentioned above is described in Figure 17a. The synthesized materials were coated on GCE and their performance was determined by employing the CV and DPV methods for the determination of ornidazole (OZ).

As we can see in Figure 17b, the BaW-based electrode demonstrated the lowest electrochemical activity, whereas the CoW-based GCE electrode showed the highest current response. Thus, the authors used CaW as the optimized material. Furthermore, the authors used different wt% of the CaW on the surface of CE-BN to further improve the electrochemical activity of the prepared composite. The authors found that 85 wt% is enough to provide better electrochemical performance for the prepared composite material (Figure 17c). In further investigations, the authors also optimized the amount of the electrode material on the surface of the GCE and the 6 μL loaded electrode demonstrated the highest electrochemical activity (Figure 17d). The $CoWO_4$/CE-BN/GCE exhibited an LOD of 0.002 μM using the DPV method with a linear range of 0.04 μM to 122.18 μM. The fabricated sensor also demonstrated excellent selectivity, repeatability, stability, repro-

ducibility, and reversibility. The real-sample recovery in lake water samples was also found to be satisfactory. Prajapati et al. [84] reported the preparation of a samarium (Sm)-doped NiO-supported BN (SmNiO@BN) composite for the sensing of acetaminophen. The synthesized SmNiO@BN was deposited on the active area of the GCE and its performance was determined towards the detection of acetaminophen using CV, DPV, and EIS methods. The authors stated that SmNiO@BN has synergistic interactions along with high surface area and more active sites for the efficient oxidation of acetaminophen, which may further provide better charge transfer, and enhanced sensing activity can be observed. The electrochemical studies demonstrated an excellent LOD of 0.43 μM along with a linear range of 0.5 μM to 13,000 μM. It was stated that constructed electrode also has decent selectivity and acceptable recovery in real samples. Karuppaiah et al. [85] reported that mesotrione (MTO) is one of the herbicides which is commonly used in agriculture but has negative influences on the environment and aquatic life. Thus, it would be worth developing an MTO sensor using simple and cost-effective strategies. In this regard, the authors developed an MTO sensor by employing spinel zinc manganese oxide ($ZnMn_2O_4$, ZMO) NPs/amine-functionalized BN (NH_2-BN) composite as an electrode modifier. The composite material was synthesized by a co-precipitation method. The ZMO NPs/NH_2-BN was coated on GCE and its sensing ability was determined by employing the CV method. The proposed electrode (ZMO NPs/NH_2-BN/GCE) exhibited an LOD of 1.5 nM and sensitivity of 1.791 μA/μM.cm^2. This MTO sensor also showed good linear ranges of 0.01 μM to 12.51 μM and 18.51 μM to 1777.51 μM for real-sample recovery in water samples. Karupppaiah et al. [86] reported the fabrication of the veterinary antibiotic drug ronidazole (RNZ). In this regard, the authors prepared a $CoCo_2O_4$ NRs/h-BN composite by employing a cetyl trimethyl ammonium bromide (CTAB)-assisted hydrothermal method followed by an ultra-sonication/stirring process. The prepared material was coated on GCE and its electrochemical performance was evaluated for the sensing of RNZ. A good LOD of 3 nM and high sensitivity of 5.845 μA/μM.cm^2 were achieved for the sensing of RNZ. Karuppusamy et al. [87] proposed the preparation of S-atom-induced electronic structure modulation of an S-SnO_2/S-hBN composite by a benign one-step vulcanization approach. Furthermore, the authors fabricated a toxic insecticide bendiocarb (BDC) sensor using the S-SnO_2/S-hBN composite as an electrode modifier and reported a good LOD of 0.285 μM and sensitivity of 0.023 μA/μM.cm^2. The fabricated sensor also demonstrated a wide linear range of 0.02 μM to 150.02 μM towards the sensing of BDC. The authors also stated that the proposed sensor has good performance for real-sample studies and stability with good reproducibility. J. S. et al. [88] reported the fabrication of solvent-exfoliated h-BNNs for the sensing of a hazardous primary azide (sodium azide, SA). The synthesized h-BNNs were deposited on GCE and its sensing activity for the determination of SA was checked by employing CV and DPV approaches. The authors reported an interesting LOD of 0.1 nM for the determination of SA. The constructed sensor was also found to be efficient for real-sample studies in tap water, groundwater, and river water samples. It is well understood that metol (MTL) is one of the most serious pollutants and possesses negative impacts on aquatic life. John et al. [89] reported the construction of an MTL sensor using a cost-effective approach. In this connection, the authors prepared a copper bismuth oxide-based composite with hBN ($CuBi_2O_4$/hBN) using a hydrothermal method-assisted ultra-sonication approach. The $CuBi_2O_4$/hBN-coated electrode demonstrated good electrochemical performance for the determination of MTL using the DPV and CV methods. The authors achieved an LOD of 0.0052 μM with sensitivity of 1.976 μA/μM.cm^2. This MTL sensor showed a linear range of 0.001 μM to 1987 μM with good recovery (97% to 99%) in pond, tap, and river water samples. Sensing performance of the various BN based electrodes are presented in Table 2.

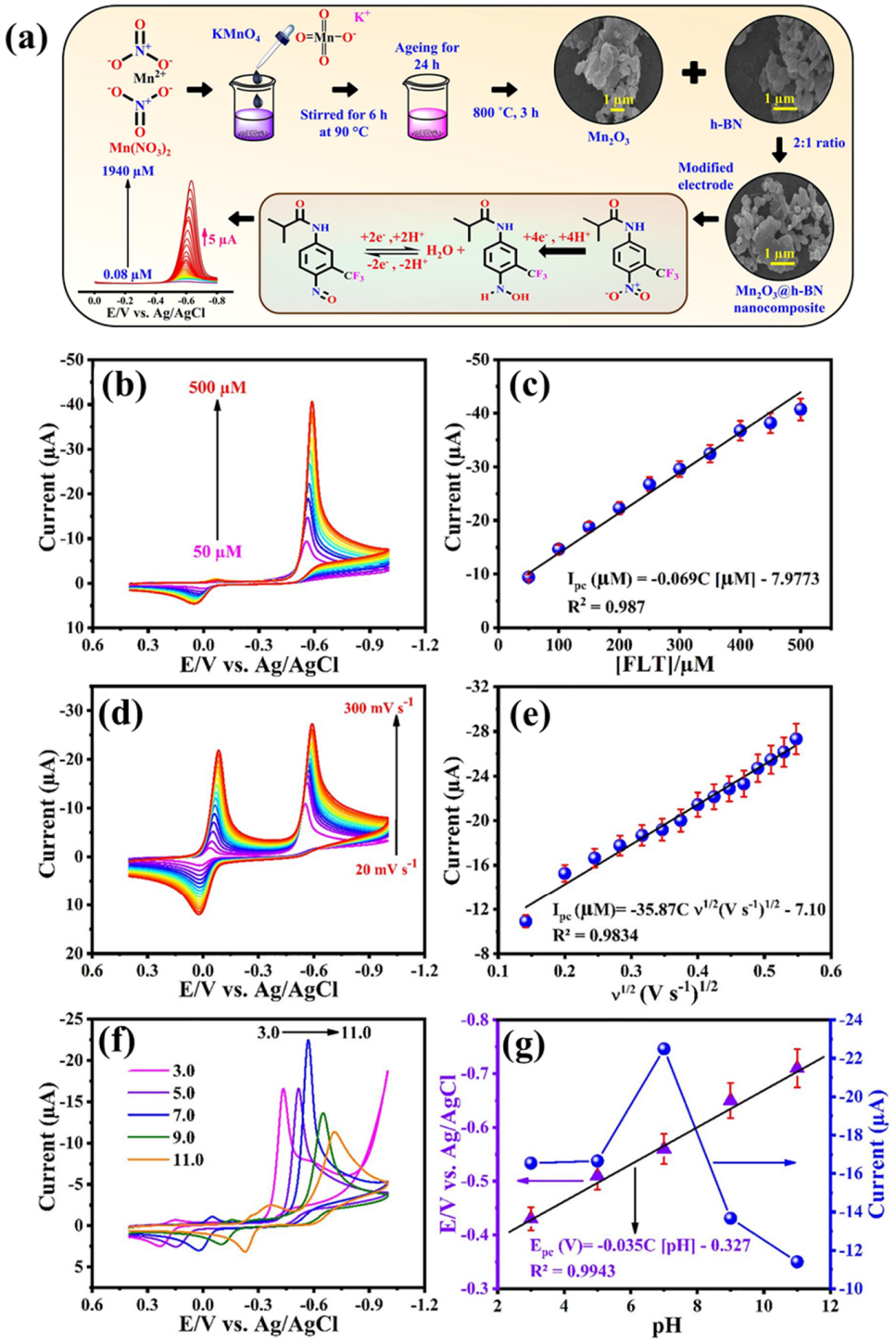

Figure 13. (**a**) Schematic picture shows synthesis of Mn_2O_3@h-BN composite for FLT sensing. (**b**) CV results for Mn_2O_3@h-BN in various amounts of FLT (50 to 500 µM) and (**c**) corresponding linear plot of current peak versus concentration. (**d**) CV results of Mn_2O_3@h-BN for 200 µM FLT at varied scan rates and (**e**) corresponding linear curve. (**f**) CV results of Mn_2O_3@h-BN for 200 µM FLT in different pH and (**g**) corresponding plot between peak current and pH. Reproduced with permission [71].

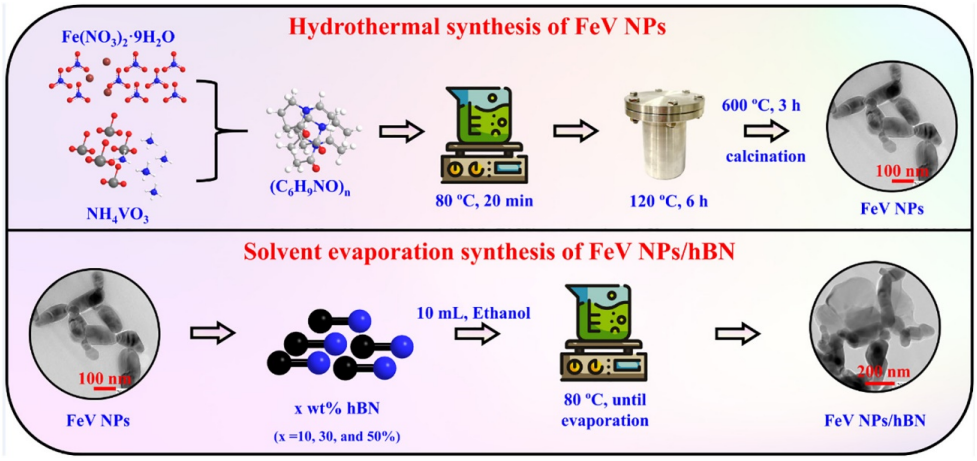

Figure 14. Schematic illustration of the synthesis of FeV and FeV NPs/hBN composite. Reproduced with permission [73].

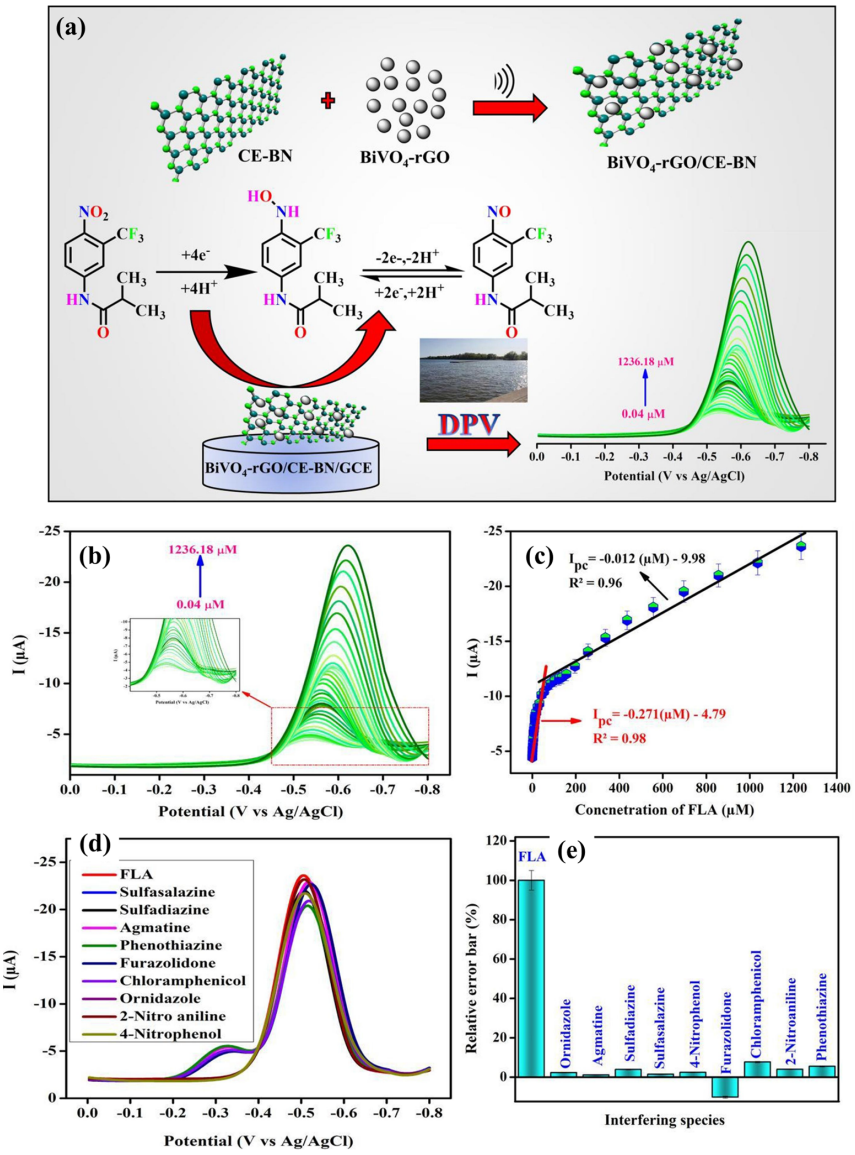

Figure 15. (**a**) Schematic graph for the fabrication of $BiVO_4$-rGO/CE-BN/GCE for sensing application. (**b**) DPVs of $BiVO_4$-rGO/CE-BN/GCE for various amounts of FLA and (**c**) corresponding linear calibration curve. (**d**) Selectivity test and corresponding (**e**) error bar for interfering species. Reproduced with permission [78].

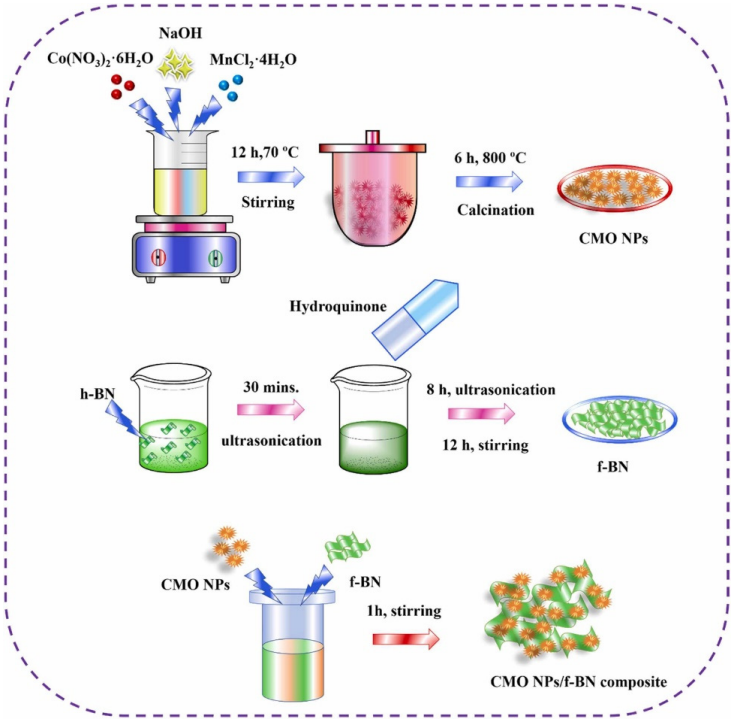

Figure 16. Schematic graphs show the synthetic procedure for the CMO NPs/f-CN composite. Reproduced with permission [82].

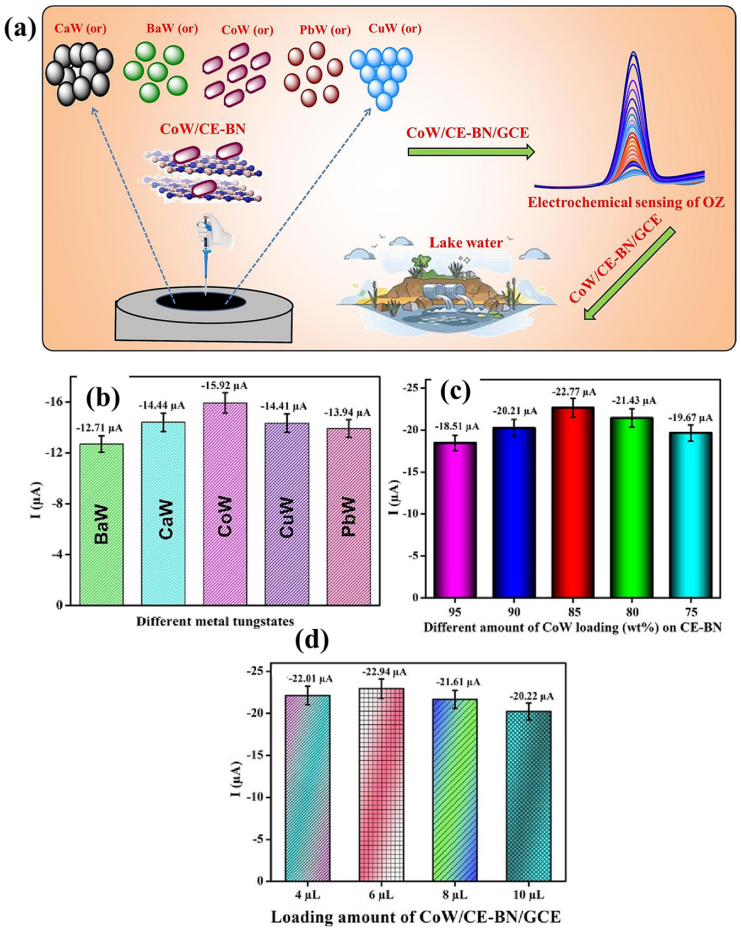

Figure 17. (**a**) Schematic graph for synthetic procedure. (**b**) CV response for different electrodes. (**c**) Effects of different wt% of CoW on CE-BN. (**d**) Effects of loading amounts of CoW/CE-BN/GCE. Reproduced with permission [83].

Table 2. Electrochemical sensing performance of the various BN composite-based sensors.

Electrode Material	Sensing Method	LOD (μM)	Linear Range (μM)	Target Analyte	Real Sample	Refs.
Cu-h-BNNS	DPV	0.03	0.09 to 9853.45	Nitrite	River water	[61]
BNNS-Au NPs	SWV	1.7×10^{-6}	0.000005 to 0.0012 and 0.02 to 10	Flavonoid luteolin	Dried peanut shells and Perilla leaves	[62]
MIP/GQDs/ 2D-hBN	DPV	0.2×10^{-6}	1.0×10^{-6} to 0.01	Serotonin	Urine	[63]
2D-hBN/ f-MWCNTs	DPV	0.1×10^{-6}	1.0×10^{-6} to 0.01	PEA	Urine	[64]
2D-hBN/ f-MWCNTs	DPV	0.1×10^{-6}	1.0×10^{-6} to 0.01	RAC	Urine	[64]
2D-hBN/ f-MWCNTs	DPV	0.1×10^{-6}	1.0×10^{-6} to 0.01	SAL	Urine	[64]
D-h-BN	DPV	0.033	0.1 to 30	Phenol	Lake water	[67]
D-h-BN	DPV	0.0033	0.0 to 30	4-AP	Tap and lake water	[67]
Pd NPs/BN HJ	LSV	0.003	0.01 to 210	PXL	River	[68]
h-BN/HNTs	i-t	0.001	0.009 to 173.0	Furazolidone	Milk and egg	[69]
BN/graphene	i-t	0.42	1 to 1000	Nicotine	Tobacco	[70]
Mn_2O_3@h-BN	DPV	0.0085	0.08 to 1940	Flutamide	Urine	[71]
FeV NPs/30 h-BN	DPV	0.004	0.04 to 2222.1	CPZ	Urine and human serum	[73]
SrP/h–BN	i-t	0.0003	0.001 to 150 and 170 to 337	DA	Urine	[74]
g-C_3N_4/BN(1:1)	DPV/i-t	0.00923	0.02 to 0.08 and 009 to 0.17	HQ	Tap and industrial wastewater	[75]
Bi_2O_3/h-BN	DPV	0.009	0.04–87	FTM	River	[76]
YO/BN	DPV	0.006	0.05 to 235	DA	Human serum	[77]
	i-t	0.0003	0.008 to 241	DA		[77]
$BiVO_4$-rGO/CE-BN	DPV	0.011	0.04 to 102	FLT	Lake water	[78]
BN/Uricase/Nafion	CA	0.14	5 to 3000	Uric acid	Human serum	[79]
SnSe/h-BN	CV/i-t	0.00034	0.001 to 12.12 and 15.2 to 342.2	Nitrofurazone	Urine and water	[80]

4. Conclusions and Perspectives

In this section, it can be concluded that BN has excellent properties and can be used for the development of energy storage devices as well as electrochemical sensors. The reported findings demonstrate that pristine BN does not have sufficient ability for use in practical applications. Thus, BN-based hybrid composites have been prepared and used for the construction of SCs and electrochemical sensors, as mentioned in this review article. The BN-based composites demonstrated decent specific capacitance and stability for long-term applications, as shown in Table 1. It was observed from the reported studies that h-BN has attracted the scientific community due to its excellent electrical insulation, chemical inertness, highly thermally conductive nature, and better optical transparency. Thus, it is clear

that BN-based composites (SAA@GBN2@Ni, $CoMoO_4$@hBN, and h-BN/rGO/CdS@PPy) are promising electrode materials for the development of energy storage devices. In previous studies, BN-based composites were also used as electrode modifiers for the sensing of nitrite, flavonoid luteolin, serotonin, PEA, RAC, SAL, phenol, 4-AP, PXL, CPZ, HQ, DA, uric acid, FTM, FLT, nitrofurazone, furazolidone, and nicotine, etc. The reported electrochemical sensors showed that i-t and DPV are two efficient and highly sensitive techniques for the determination of various analytes. BN-based composites demonstrated excellent performance for energy storage and electrochemical sensing applications. However, some challenges still need to be addressed for their practical application. These challenges include aggregation of BN, limited charge storage capacity, and interfacial compatibility. The performance of BN-based composites can be improved by incorporating MXene-based composites with BN, layered hydroxides, and polymers to form the hybrid composites for long-term electrochemical applications. In the case of stability, nanostructured or BN-based material-modified electrodes exhibit cyclic stability for up to 10,000 or 20,000 cycles in the laboratory under optimized and controlled conditions. However, these data might not be directly relevant for real-world scenarios due to the differentiation between real-world and laboratory conditions. Researchers used ideal conditions for experiments which may not reflect the variable or harsh environment conditions (such as temperature, mechanical stress, and humidity) of real-world scenarios. Thus, it is required to bridge the gap by deep studies and discussions for practical applications of electrochemical devices.

Author Contributions: Conceptualization, K.A. and T.H.O.; writing—original draft preparation, K.A.; writing—review and editing, K.A. and T.H.O. All authors have read and agreed to the published version of the manuscript.

Funding: This research received no external funding.

Conflicts of Interest: The authors declare no conflicts of interest.

References

1. Gajdzik, B.; Wolniak, R.; Nagaj, R.; Žuromskaitė-Nagaj, B.; Grebski, W.W. The Influence of the Global Energy Crisis on Energy Efficiency: A Comprehensive Analysis. *Energies* **2024**, *17*, 947. [CrossRef]
2. Bollino, C.A.; Asdrubali, F.; Polinori, P.; Bigerna, S.; Micheli, S.; Guattari, C.; Rotili, A. A Note on Medium- and Long-Term Global Energy Prospects and Scenarios. *Sustainability* **2017**, *9*, 833. [CrossRef]
3. Al-Ezzi, A.S.; Ansari, M.N.M. Photovoltaic Solar Cells: A Review. *Appl. Syst. Innov.* **2022**, *5*, 67. [CrossRef]
4. Czagany, M.; Hompoth, S.; Keshri, A.K.; Pandit, N.; Galambos, I.; Gacsi, Z.; Baumli, P. Supercapacitors: An Efficient Way for Energy Storage Application. *Materials* **2024**, *17*, 702. [CrossRef]
5. Liu, W.; Sun, X.; Yan, X.; Gao, Y.; Zhang, X.; Wang, K.; Ma, Y. Review of Energy Storage Capacitor Technology. *Batteries* **2024**, *10*, 271. [CrossRef]
6. AlZohbi, G. An Overview of Hydrogen Energy Generation. *ChemEngineering* **2024**, *8*, 17. [CrossRef]
7. Olabi, A.G.; Sayed, E.T. Developments in Hydrogen Fuel Cells. *Energies* **2023**, *16*, 2431. [CrossRef]
8. Yuan, M.; Zhang, X.; Wang, J.; Zhao, Y. Recent Progress of Energy-Storage-Device-Integrated Sensing Systems. *Nanomaterials* **2023**, *13*, 645. [CrossRef]
9. Teli, A.M.; Beknalkar, S.A.; Lee, Y.R.; Shin, J.C. Novel one-step synthesis for 3-D four-pointed micro-star of quaternary metal (Mo–V–Mn–Ag) oxide electrode for asymmetric supercapacitor. *Ceram. Int.* **2022**, *48*, 36249–36257. [CrossRef]
10. Gan, Z.; Ren, X.; Liu, M.; Sun, M.; Shen, W.; Li, Z. Advances in design of copper-based nanostructures and nanocomposites for high-performance supercapacitors. *J. Energy Storage* **2024**, *99*, 113383. [CrossRef]
11. Balasubramaniam, S.; Mohanty, A.; Balasingam, S. Comprehensive insight into the mechanism, material selection and performance evaluation of supercapatteries. *Nano-Micro Lett.* **2020**, *12*, 85. [CrossRef] [PubMed]
12. Abed, M.; Rezaee Roknabadi, M.; Nakhaei Pour, A. Improvement of physical properties of zinc oxide and activated carbon nanocomposite for use in supercapacitor electrode. *J. Mater. Sci. Mater. Electron.* **2024**, *35*, 1328. [CrossRef]
13. Patil, R.B.; Yadav, A.D.; Kanamadi, C.M.; Patil, S.P. Electrochemical advancements: MnO_2-based electrode materials for supercapacitors. *Ionics* **2024**. [CrossRef]

14. Demirel, S.; Nas, M.S.; Kocyigit, A.; Calimli, M.H.; Alma, M.H. High capacitive pt and NiO_x loaded supercapacitors with commercial and green synthesized carbon-based materials. *J. Mater. Sci. Mater. Electron.* **2024**, *35*, 174. [CrossRef]
15. Sarkar, A.; Taguessong, B.C.; Chen, X.G.; Sarkar, D.K. Supercapacitor properties of $Cu_2O/Cu(OH)_2$ composite thin films deposited on nickel foam using pulse reverse potential electrodeposition. *J. Mater. Sci. Mater. Electron.* **2024**, *35*, 1901. [CrossRef]
16. Babu, C.R.; Avani, A.V.; Shaji, S.; Anila, E.I. Electrochemical characteristics of Co_3O_4 nanoparticles synthesized via the hydrothermal approach for supercapacitor applications. *J. Solid State Electrochem.* **2024**, *28*, 2203–2210. [CrossRef]
17. Sohail, A.; Aalim, M.; Ahmad, R.; Altaf, U.; Shah, M.A.; Majid, K. Enhanced electrochemical characteristics of Mn Al-co-doped SnO_2 nanostructures for high-performance supercapacitor application. *J. Mater. Sci. Mater. Electron.* **2024**, *35*, 1302. [CrossRef]
18. Thejasree, K.; Aparna, M.L.; Ghosh, T.K.; Mishra, V.; Reddy, K.R.; Rao, G.R. Ball-milled MoO_3@$NiCo_2Se_4$ composite for supercapacitor electrode. *J. Solid State Electrochem.* **2024**. [CrossRef]
19. Muslu, E.; Eren, E.; Oksuz, A.U. Research progress on flexible WO_3 based thin film electrodes for supercapacitor applications: A comprehensive review. *Emergent Mater.* **2024**. [CrossRef]
20. Ouda, E.; Yousf, N.; Magar, H.S.; Hassan, R.Y.; Duraia, E.S.M. Electrochemical properties of MnO_2-based carbon nanomaterials for energy storage and electrochemical sensing. *J. Mater. Sci. Mater. Electron.* **2023**, *34*, 731. [CrossRef]
21. Baranwal, J.; Barse, B.; Gatto, G.; Broncova, G.; Kumar, A. Electrochemical Sensors and Their Applications: A Review. *Chemosensors* **2022**, *10*, 363. [CrossRef]
22. Singh, K.; Maurya, K.K.; Malviya, M. Review of Electrochemical Sensors and Biosensors Based on First-Row Transition Metals, Their Oxides, and Noble Metals Nanoparticles. *J. Anal. Test.* **2024**, *8*, 143–159. [CrossRef]
23. Negahdary, M.; Ameku, W.A.; Santos, B.G.; Lima, I.S.; de Oliveira, T.G.; França, M.C.; Angnes, L. Recent electrochemical sensors and biosensors for toxic agents based on screen-printed electrodes equipped with nanomaterials. *Microchem. J.* **2023**, *185*, 108281. [CrossRef]
24. Patil, V.B.; Ilager, D.; Tuwar, S.M.; Mondal, K.; Shetti, N.P. Nanostructured ZnO-Based Electrochemical Sensor with Anionic Surfactant for the Electroanalysis of Trimethoprim. *Bioengineering* **2022**, *9*, 521. [CrossRef]
25. Zhu, C.; Wu, Q.; Yuan, F.; Liu, J.; Wang, D.; Zhang, Q. Novel Electrochemical Sensor Based on MnO_2 Nanowire Modified Carbon Paper Electrode for Sensitive Determination of Tetrabromobisphenol A. *Chemosensors* **2023**, *11*, 482. [CrossRef]
26. Mathad, A.; Korgaonkar, K.; Jaldappagari, S.; Kalanur, S. Ultrasensitive Electrochemical Sensor Based on SnO_2 Anchored 3D Porous Reduced Graphene Oxide Nanostructure Produced via Sustainable Green Protocol for Subnanomolar Determination of Anti-Diabetic Drug, Repaglinide. *Chemosensors* **2023**, *11*, 50. [CrossRef]
27. Zhao, K.; Zhang, Z.; Zhou, Y.; Lin, X. Ag-CeO_2 Based on Electrochemical Sensor for High-Efficient On-Site Detection of Nitrite in Aquaculture Water and Beverages. *Molecules* **2024**, *29*, 2644. [CrossRef]
28. Shepa, J.; Šišoláková, I.; Vojtko, M.; Trnková, L.; Nagy, G.; Maskaľová, I.; Oriňak, A.; Oriňaková, R. NiO Nanoparticles for Electrochemical Insulin Detection. *Sensors* **2021**, *21*, 5063. [CrossRef]
29. Zou, J.; Liu, J.; Peng, G.; Huang, H.; Wang, L.; Lu, L.; Gao, Y.; Hu, D.; Chen, S. An Electrochemical Sensor Based on a Porous Biochar/Cuprous Oxide (BC/Cu_2O) Composite for the Determination of Hg(II). *Molecules* **2023**, *28*, 5352. [CrossRef]
30. Thamilselvan, A.; Dang, T.V.; Kim, M.I. Highly Conductive Peroxidase-like Ce-MoS_2 Nanoflowers for the Simultaneous Electrochemical Detection of Dopamine and Epinephrine. *Biosensors* **2023**, *13*, 1015. [CrossRef]
31. Ogawa, S.; Fukushima, S.; Shimatani, M. Hexagonal Boron Nitride for Photonic Device Applications: A Review. *Materials* **2023**, *16*, 2005. [CrossRef] [PubMed]
32. Alamro, A.; Balbaied, T. Boron Nitride Nanostructures (BNNs) Within Metal–Organic Frameworks (MOFs): Electrochemical Platform for Hydrogen Sensing and Storage. *Analytica* **2024**, *5*, 599–618. [CrossRef]
33. Dobrzhinetskaya, L.F.; Wirth, R.; Yang, J.; Green, H.W.; Hutcheon, I.D.; Weber, P.K.; Grew, E.S. Qingsongite, natural cubic boron nitride: The first boron mineral from the Earth's mantle. *Am. Mineral.* **2014**, *99*, 764–772. [CrossRef]
34. Maheshwaran, G.; Pandi, P.; Suganya, S.; Kumar, B.A.; Ramalingam, G.; Prabhu, M.R.; Sudhahar, S. Fabrication of self charging supercapacitor based on two dimensional bismuthene-graphitic carbon nitride nanocomposite powered by dye sensitized solar cells. *J. Energy Storage* **2022**, *56*, 105900. [CrossRef]
35. Sasikumar, S.; Rajaram, A. Unveiling the cobalt vanadate supported hexagonal boron nitride nanocomposite for photocatalytic wastewater treatment: Enhanced degradation of dyes, antibiotics, and real industrial wastewater. *Mater. Sci. Semicond. Process.* **2024**, *177*, 108407. [CrossRef]
36. Ribag, K.; Houmad, M.; Benyoussef, A.; Kenz, A. Strain and pH enhanced the photocatalytic properties and hydrogen production of tetragonal boron nitride. *Comput. Theor. Chem.* **2024**, *1241*, 114836. [CrossRef]
37. Alfalasi, W.; Othman, W.; Hussain, T.; Tit, N. Multifunctionality of vacancy-induced boron nitride monolayers for metal-ion battery and hydrogen-storage applications. *Appl. Surf. Sci.* **2025**, *685*, 162025. [CrossRef]
38. Liu, F.; Gao, D.; Wang, F.; Shen, P.; Liu, Y.; Zhang, S.; Li, Y.; Zhang, J.; Xue, Y.; Tang, C. Boron carbon nitride as efficient oxygen reduction reaction support. *J. Colloid Interface Sci.* **2024**, *673*, 901–908. [CrossRef]

39. Duhduh, A.A.; Saraswat, S.K.; Lagum, A.A.; Al-Ma'abreh, A.M.; Alawideh, S.; Alamri, S.; Rajhi, A.A.; Kadhim, M.M. Exploring Ni-doped boron carbide nanotubes: Structural and electronic properties for proton-exchange membrane fuel cells. *Inorg. Chem. Commun.* **2023**, *155*, 111110. [CrossRef]
40. Sun, D.; Sun, Z.; Yang, D.; Jiang, X.; Tang, J.; Wang, X. Advances in boron nitride-based materials for electrochemical energy storage and conversion. *EcoEnergy.* **2023**, *1*, 375–404. [CrossRef]
41. Gao, T.; Gong, L.-J.; Wang, Z.; Yang, Z.-K.; Pan, W.; He, L.; Zhang, J.; Ou, E.-C.; Xiong, Y.; Xu, W. Boron nitride/reduced graphene oxide nanocomposites as supercapacitors electrodes. *Mater. Lett.* **2015**, *159*, 54–57. [CrossRef]
42. Saha, S.; Samanta, P.; Murmu, N.C.; Kim, N.H.; Kuila, T.; Lee, J.H. Electrochemical functionalization and in-situ deposition of the SAA@rGO/h-BN@Ni electrode for supercapacitor applications. *J. Ind. Eng. Chem.* **2017**, *52*, 321–330. [CrossRef]
43. Saha, S.; Jana, M.; Samanta, P.; Murmu, N.C.; Kim, N.H.; Kuila, T.; Lee, J.H. Investigation of band structure and electrochemical properties of h-BN/rGO composites for asymmetric supercapacitor applications. *Mater. Chem. Phys.* **2017**, *190*, 153–165. [CrossRef]
44. Patil, I.M.; Kapse, S.; Parse, H.; Thapa, R.; Andersson, G.; Kakade, B. 2D/3D heterostructure of h-BN/reduced graphite oxide as a remarkable electrode Material for supercapacitor. *J. Power Sources* **2020**, *479*, 229092. [CrossRef]
45. Lee, J.W.; Kshetri, T.; Park, K.R.; Kim, N.H.; Park, O.-K.; Lee, J.H. Covalently bonded boron nitride quantum dot and reduced graphene oxide composite electrode for highly efficient supercapacitors. *Compos. Part B Eng.* **2021**, *222*, 109089. [CrossRef]
46. Rajendran, J.; Reshetilov, A.N.; Sundramoorthy, A.K. Preparation of hybrid paper electrode based on hexagonal boron nitride integrated graphene nanocomposite for free-standing flexible supercapacitors. *RSC Adv.* **2021**, *11*, 3445–3451. [CrossRef]
47. Hassan, M.; Gondal, M.A.; Cevik, E.; Qahtan, T.F.; Bozkurt, A.; Dastageer, M.A. High performance pliable supercapacitor fabricated using activated carbon nanospheres intercalated into boron nitride nanoplates by pulsed laser ablation technique. *Arab. J. Chem.* **2020**, *13*, 6696–6707. [CrossRef]
48. Li, T.; Jiao, X.; You, T.; Dai, F.; Zhang, P.; Yu, F.; Hu, L.; Ding, L.; Zhang, L.; Wen, Z.; et al. Hexagonal boron nitride nanosheet/carbon nanocomposite as a high-performance cathode material towards aqueous asymmetric supercapacitors. *Ceram. Int.* **2019**, *45*, 4283–4289. [CrossRef]
49. Gunday, S.T.; Cevik, E.; Yusuf, A.; Bozkurt, A. Nanocomposites composed of sulfonated polysulfone/hexagonal boron nitride/ionic liquid for supercapacitor applications. *J. Energy Storage* **2019**, *21*, 672–679. [CrossRef]
50. Barai, H.R.; Rahman, M.; Rahim, A.; Joo, S.W. α-MnO_2 nanorod/boron nitride nanoplatelet composites for high-performance nanoscale dielectric pseudocapacitor applications. *J. Ind. Eng. Chem.* **2019**, *79*, 115–123. [CrossRef]
51. Lin, L.; Chen, S.; Qi, X.; Yao, J.; Meng, L.; Chen, W. h-BN doped β-MnO_2 nanobelts composite as superior electrode materials for supercapacitors. *Mater. Lett.* **2022**, *328*, 133209. [CrossRef]
52. Maity, C.K.; Goswami, N.; Verma, K.; Sahoo, S.; Nayak, G.C. A facile synthesis of boron nitride supported zinc cobalt sulfide nano hybrid as high-performance pseudocapacitive electrode material for asymmetric supercapacitors. *J. Energy Storage* **2020**, *32*, 101993. [CrossRef]
53. Panicker, N.J.; Ajayan, P.M.; Sahu, P.P. Band-gap tuned hexagonal-boron nitride/reduced graphene oxide superlattice wrapped cadmium sulfide/Polypyrrole nanocomposite as an efficient supercapacitor electrode material. *J. Energy Storage* **2022**, *56*, 105901. [CrossRef]
54. Maity, C.K.; De, S.; Acharya, S.; Siddiki, S.H.; Sahoo, S.; Verma, K.; Thakur, V.K.; Nayak, G.C. Copper oxide stabilized oxy-functionalized boron nitride-carbon nanotube nanohybrid: An ultra-stable electrode for flexible asymmetric supercapacitor device in ionic electrolyte. *J. Energy Storage* **2022**, *56*, 105928. [CrossRef]
55. Sakaray, M.; Chidurala, S.C. Optimization of ternary composite @PANI/MoO_3/h-BN and its electrochemical evaluation as an electrode material for supercapacitor application. *Synth. Met.* **2023**, *298*, 117448. [CrossRef]
56. Maity, C.K.; De, S.; Panigrahi, A.; Acharya, S.; Verma, K.; Kim, M.J.; Nayak, G.C. Aerosol derived carbon dots decorated boron nitride supported Zn-doped MoS_2 for high performing flexible asymmetric supercapacitor. *Compos. Part B Eng.* **2023**, *264*, 110887. [CrossRef]
57. Rahman, M.; Hossen, R.; Alam, I.; Rahman, H.; Faruk, O.; Nurbas, M.; Rahman, M.M.; Khan, M.M.R. Synthesis of hexagonal boron nitride based PANI/h-BN and PANI-PPy/h-BN nanocomposites for efficient supercapacitors. *J. Alloys Compd.* **2023**, *947*, 169471. [CrossRef]
58. Zhao, Y.; Ghanem, M.A.; Reddy, G.R.; Joo, S.W. Probing structural and electrochemical properties of a 2D $CoMoO_4$@hBN nanocomposite as pseudocapacitive electrode for high-performance supercapacitors. *Ceram. Int.* **2024**, *50*, 55330–55341. [CrossRef]
59. Dhamodharan, K.; Singh, A.K. Coupled interaction of exfoliated hexagonal boron nitride nanosheets decorated with MoS_2 nanoflowers to enrich electrochemical activities for hybrid supercapacitor applications. *J. Alloys Compd.* **2024**, *997*, 174732.
60. Sharma, C.; Vanishree, P.; Rani, B.; Lohia, N.; Swati, G.; Srivastava, R.; Sharma, S.N. Electrochemical properties of two-dimensional hexagonal boron nitride nanosheets prepared by hydrothermal method. *Electrochim. Acta* **2023**, *463*, 142848. [CrossRef]
61. Zhang, Y.; Xia, Z.; Li, Q.; Gui, G.; Zhao, G.; Luo, S.; Yang, M.; Lin, L. Copper/hexagonal Boron Nitride Nanosheet Composite as an Electrochemical Sensor for Nitrite Determination. *Int. J. Electrochem. Sci.* **2018**, *13*, 5995–6004. [CrossRef]

62. Fu, L.; Liu, Z.; Huang, Y.; Lai, G.; Zhang, H.; Su, W.; Yu, J.; Wang, A.; Lin, C.-T.; Yu, A. Square wave voltammetric quantitative determination of flavonoid luteolin in peanut hulls and Perilla based on Au NPs loaded boron nitride nanosheets. *J. Electroanal. Chem.* **2018**, *817*, 128–133. [CrossRef]
63. Yola, M.L.; Atar, N. A novel detection approach for serotonin by graphene quantum dots/two-dimensional (2D) hexagonal boron nitride nanosheets with molecularly imprinted polymer. *Appl. Surf. Sci.* **2018**, *458*, 648–655. [CrossRef]
64. Yola, M.L.; Atar, N. Simultaneous determination of β-agonists on hexagonal boron nitride nanosheets/multi-walled carbon nanotubes nanocomposite modified glassy carbon electrode. *Mater. Sci. Eng. C* **2019**, *96*, 669–676. [CrossRef]
65. Hatamluyi, B.; Hashemzadeh, A.; Darroudi, M. A novel molecularly imprinted polymer decorated by CQDs@HBNNS nanocomposite and UiO-66-NH_2 for ultra-selective electrochemical sensing of Oxaliplatin in biological samples. *Sens. Actuators B Chem.* **2020**, *307*, 127614. [CrossRef]
66. Karimi-Maleh, H.; Karimi, F.; Malekmohammadi, S.; Zakariae, N.; Esmaeili, R.; Rostamnia, S.; Yola, M.L.; Atar, N.; Movaghgharnezhad, S.; Rajendran, S.; et al. An amplified voltammetric sensor based on platinum nanoparticle/polyoxometalate/two-dimensional hexagonal boron nitride nanosheets composite and ionic liquid for determination of N-hydroxysuccinimide in water samples. *J. Mol. Liq.* **2020**, *310*, 113185. [CrossRef]
67. Shen, Y.; Yan, H.; Guo, H.; Long, Y.; Li, W. Defect-rich hexagonal boron nitride for the simultaneous determination of 4-aminophenol and phenol. *Sens. Actuators B Chem.* **2020**, *303*, 127248. [CrossRef]
68. Renganathan, V.; Balaji, R.; Chen, S.-M.; Kokulnathan, T. Coherent design of palladium nanostructures adorned on the boron nitride heterojunctions for the unparalleled electrochemical determination of fatal organophosphorus pesticides. *Sens. Actuators B Chem.* **2020**, *307*, 127586. [CrossRef]
69. Kokulnathan, T.; Wang, T.-J.; Thangapandian, M.; Alaswad, S.O. Synthesis and characterization of hexagonal boron nitride/halloysite nanotubes nanocomposite for electrochemical detection of furazolidone. *Appl. Clay Sci.* **2020**, *187*, 105483. [CrossRef]
70. Jerome, R.; Sundramoorthy, A.K. Preparation of hexagonal boron nitride doped graphene film modified sensor for selective electrochemical detection of nicotine in tobacco sample. *Anal. Chim. Acta* **2020**, *1132*, 110–120. [CrossRef]
71. Kesavan, G.; Chen, S.-M. Highly sensitive manganese oxide/hexagonal boron nitride nanocomposite: An efficient electrocatalyst for the detection of anti-cancer drug flutamide. *Microchem. J.* **2021**, *163*, 105906. [CrossRef]
72. Öndeş, B.; Evli, S.; Uygun, M.; Uygun, D.A. Boron nitride nanosheet modified label-free electrochemical immunosensor for cancer antigen 125 detection. *Biosens. Bioelectron.* **2021**, *191*, 113454. [CrossRef] [PubMed]
73. Kesavan, G.; Gopi, P.K.; Chen, S.-M.; Vinothkumar, V. Iron vanadate nanoparticles supported on boron nitride nanocomposite: Electrochemical detection of antipsychotic drug chlorpromazine. *J. Electroanal. Chem.* **2021**, *882*, 114982. [CrossRef]
74. Baby, J.N.; Sriram, B.; Hsu, Y.-F.; Wang, S.-F.; Bartholomew, R.; George, M. Rational incorporation of strontium pyrophosphate/hexagonal boron nitride composite for trace level electrochemical sensing of dopamine. *Microchem. J.* **2022**, *183*, 108067. [CrossRef]
75. Harikrishnan, K.; Singh, G.; Kushwaha, A.; Singh, V.P.; Gaur, U.K.; Sharma, M. 2D/2D heterojunction of graphitic carbon nitride and hexagonal boron nitride nanosheets mediated electrochemical detection of hazardous hydroquinone with high selectivity and sensitivity. *J. Environ. Chem. Eng.* **2022**, *10*, 108717. [CrossRef]
76. Kokulnathan, T.; Vishnuraj, R.; Wang, T.-J.; Kumar, E.A.; Pullithadathil, B. Heterostructured bismuth oxide/hexagonal-boron nitride nanocomposite: A disposable electrochemical sensor for detection of flutamide. *Ecotoxicol. Environ. Saf.* **2021**, *207*, 111276. [CrossRef]
77. Kokulnathan, T.; Wang, T.-J.; Kumar, E.A.; Duraisamy, N.; Lee, A.-T. An electrochemical platform based on yttrium oxide/boron nitride nanocomposite for the detection of dopamine. *Sens. Actuators B Chem.* **2021**, *349*, 130787. [CrossRef]
78. Bhuvaneswari, C.; Palpandi, K.; Amritha, B.; Paunkumar, P.; Priya, R.L.; Raman, N.; Babu, S.G. Conniving for the first time of $BiVO_4$–rGO/CE-BN and its potential as enhanced electrochemical sensing of non-steroidal anti-androgen drug. *Microchem. J.* **2023**, *184*, 108174. [CrossRef]
79. Öndeş, B.; Sunna, Ç.; Kilimci, U.; Uygun, M.; Uygun, D.A. Boron nitride nanosheet modified amperometric biosensor for uric acid determination. *Microchem. J.* **2023**, *194*, 109240. [CrossRef]
80. Thirumalraj, B.; Sriram, B.; Muthukutty, B.; Zheng, L.; Wang, S.-F.; Choe, H.; Kwon, K. Layered metal chalcogenide of SnSe nanosheets integrated with 2D-hexagonal boron nitride for accurate and low-level detection of nitrofurazone. *Chem. Eng. J.* **2023**, *455*, 140521. [CrossRef]
81. Habibi, B.; Pashazadeh, A.; Pashazadeh, S.; Saghatforoush, L.A. Copper/zeolitic imidazolate framework-8 integrated by boron nitride as an electrocatalyst at the glassy carbon electrode to sensing of the clopidogrel. *J. Solid State Chem.* **2023**, *323*, 123982. [CrossRef]
82. Jeyaraman, A.; Karuppaiah, B.; Chen, S.M.; Huang, Y.-C. Development of mixed spinel metal oxide (Co-Mn-O) integrated functionalized boron nitride: Nanomolar electrochemical detection of herbicide diuron. *Colloids Surf. A Physicochem. Eng. Asp.* **2023**, *666*, 131278. [CrossRef]

83. Bhuvaneswari, C.; Babu, S.G. Scheming the best metal tungstate laden on boron nitride: Budding en route for electrochemical sensing of ornidazole. *Microchem. J.* **2023**, *193*, 109120. [CrossRef]
84. Prajapati, J.; Singh, A.K.; Gautam, R.K.; Agrahari, S.; Chatterjee, D.; Tiwari, I. Samarium doped nickel oxide supported on 2D-hexagonal boron nitride nanosheets for electrochemical sensing of Acetaminophen. *Mater. Res. Bull.* **2023**, *166*, 112329. [CrossRef]
85. Karuppaiah, B.; Anupriya, J.; Chen, S.M.; Park, S.J. An emergent electrochemical sensor based on spinel zinc manganese oxide decorated on amine-functionalized boron nitride for enhanced electrochemical determination of herbicide mesotrione. *Process Saf. Environ. Prot.* **2023**, *176*, 292–303. [CrossRef]
86. Karupppaiah, B.; Jeyaraman, A.; Chen, S.-M.; Huang, Y.-C. Development of highly sensitive electrochemical sensor for antibiotic drug ronidazole based on spinel cobalt oxide nanorods embedded with hexagonal boron nitride. *Electrochim. Acta* **2023**, *446*, 142008. [CrossRef]
87. Karuppusamy, N.; Jeyaraman, A.; Chen, S.-M.; Manavalan, S.; Jung, S.M. Electronic structure modulation on SnO_2 and hexagonal boron nitride with sulfur atom for effective electrochemical sensing of Bendiocarb. *Chem. Eng. J.* **2023**, *475*, 145834. [CrossRef]
88. Arya Nair, J.S.; Sandhya, K.Y. Nanomolar level electrochemical sensing of explosive material sodium azide by a hexagonal boron nitride modified glassy carbon electrode. *Mater. Adv.* **2024**, *5*, 3177–3185.
89. John, A.J.V.; Disouza, F.P.D.; Chen, T.-W.; Chen, S.-M.; Alagarsamy, S.; Liou, W.-C.; Al-onazi, W.A.; Algarni, T.S.; Elshikh, M.S. Spinel $CuBi_2O_4$ integrated with boron nitride hexagons for a sensitive electro-analytical quantification of environmental organic pollutants. *Process Saf. Environ. Prot.* **2024**, *188*, 1246–1255. [CrossRef]

Disclaimer/Publisher's Note: The statements, opinions and data contained in all publications are solely those of the individual author(s) and contributor(s) and not of MDPI and/or the editor(s). MDPI and/or the editor(s) disclaim responsibility for any injury to people or property resulting from any ideas, methods, instructions or products referred to in the content.